JVI Journals.ASM.org

Oropouche Virus Infection and Pathogenesis Are Restricted by MAVS, IRF-3, IRF-7, and Type I Interferon Signaling Pathways in Nonmyeloid Cells

Jose Luiz Proenca-Modena,[a,e] Renata Sesti-Costa,[b,f] Amelia K. Pinto,[a] Justin M. Richner,[a] Helen M. Lazear,[a] Tiffany Lucas,[a] Jennifer L. Hyde,[a] Michael S. Diamond[a,b,c,d]

Departments of Medicine,[a] Pathology & Immunology,[b] and Molecular Microbiology[c] and Center for Human Immunology and Immunotherapy Programs,[d] Washington University School of Medicine, St. Louis, Missouri, USA; Department of Genetics, Evolution and Bioagents, Institute of Biology, University of Campinas (UNICAMP), Campinas, São Paulo, Brazil[e]; Department of Biochemistry and Immunology, University of São Paulo (USP) Ribeirão Preto School of Medicine, São Paulo, Brazil[f]

ABSTRACT

Oropouche virus (OROV) is a member of the *Orthobunyavirus* genus in the *Bunyaviridae* family and a prominent cause of insect-transmitted viral disease in Central and South America. Despite its clinical relevance, little is known about OROV pathogenesis. To define the host defense pathways that control OROV infection and disease, we evaluated OROV pathogenesis and immune responses in primary cells and mice that were deficient in the RIG-I-like receptor signaling pathway (MDA5, RIG-I, or MAVS), downstream regulatory transcription factors (IRF-3 or IRF-7), beta interferon (IFN-β), or the receptor for type I IFN signaling (IFNAR). OROV replicated to higher levels in primary fibroblasts and dendritic cells lacking MAVS signaling, the transcription factors IRF-3 and IRF-7, or IFNAR than in wild-type (WT) cells. In mice, deletion of IFNAR, MAVS, or IRF-3 and IRF-7 resulted in uncontrolled OROV replication, hypercytokinemia, extensive liver damage, and death, whereas WT congenic animals failed to develop disease. Unexpectedly, mice with a selective deletion of IFNAR on myeloid cells (CD11c Cre^{+} *Ifnar*$^{f/f}$ or LysM Cre^{+} *Ifnar*$^{f/f}$) did not sustain enhanced disease with OROV or a selective (flox/flox) deletion La Crosse virus, a closely related encephalitic orthobunyavirus. In bone marrow chimera studies, recipient irradiated *Ifnar*$^{-/-}$ mice reconstituted with WT hematopoietic cells sustained high levels of OROV replication and liver damage, whereas WT mice reconstituted with *Ifnar*$^{-/-}$ bone marrow were resistant to disease. Collectively, these results establish a dominant protective role for MAVS, IRF-3 and IRF-7, and IFNAR in restricting OROV infection and tissue injury and suggest that IFN signaling in nonmyeloid cells contributes to the host defense against orthobunyaviruses.

IMPORTANCE

Oropouche virus (OROV) is an emerging arthropod-transmitted orthobunyavirus that causes episodic outbreaks of a debilitating febrile illness in humans in countries of South and Central America. The continued expansion of the range and number of its arthropod vectors increases the likelihood that OROV will spread into new regions. At present, the pathogenesis of OROV in humans or other vertebrate animals remains poorly understood. To define cellular mechanisms of control of OROV infection, we performed infection studies in a series of primary cells and mice that were deficient in key innate immune genes involved in pathogen recognition and control. Our results establish that a MAVS-dependent type I IFN signaling pathway has a dominant role in restricting OROV infection and pathogenesis *in vivo*.

Oropouche virus (OROV) is an arthropod-transmitted virus of the family *Bunyaviridae*, genus *Orthobunyavirus*, and serogroup Simbu. OROV has a trisegmented genome, comprised of three single-stranded negative-sense RNA segments: large (L), medium (M), and small (S). L encodes the viral RNA polymerase, M encodes the viral surface glycoproteins (Gc and Gn) and a nonstructural protein (NSm), and S encodes the nucleocapsid (N) protein and a small nonstructural protein (NSs) in overlapping reading frames (1). Although details about its cellular life cycle remain poorly characterized, OROV entry is associated with clathrin-coated pits, endosomal acidification, and membrane fusion, which facilitates nucleocapsid release into the cytoplasm (2). The receptors of OROV remain uncharacterized, although Gc is implicated in host cell attachment (3). While the precise replication strategy used by OROV has not been described, it likely occurs in the cytoplasm, similar to other bunyaviruses. Bunyavirus mRNA transcription is primed by "cap-snatching" from cytoplasmic host cellular mRNAs through activities of the viral L and N proteins (4, 5). Genome replication follows via a positive-sense strand intermediate (6). Translation of the L and S segment-encoded proteins occurs on free ribosomes in the cytoplasm, and translation of M polypeptides occurs on endoplasmic reticulum (ER)-bound ribosomes, resulting in a nascent polypeptide that is cleaved cotranslationally to generate Gn and Gc (7). Virus assembly and maturation take place in association with ER and Golgi

Received 12 January 2015 **Accepted** 18 February 2015

Accepted manuscript posted online 25 February 2015

Citation Proenca-Modena JL, Sesti-Costa R, Pinto AK, Richner JM, Lazear HM, Lucas T, Hyde JL, Diamond MS. 2015. Oropouche virus infection and pathogenesis are restricted by MAVS, IRF-3, IRF-7, and type I interferon signaling pathways in nonmyeloid cells. J Virol 89:4720–4737. doi:10.1128/JVI.00077-15.

Editor: R. W. Doms

Address correspondence to Michael S. Diamond, diamond@wusm.wustl.edu.

doi:10.1128/JVI.00077-15

membranes (8), and virion release occurs by fusion of vesicular bodies with the plasma membranes or via direct budding at the plasma membrane (7).

Since the 1960s, OROV has caused periodic outbreaks of a debilitating febrile illness, with more than 30 epidemics and 500,000 infected people in Brazil, Peru, Trinidad, Panama, and Suriname (9–11). Although OROV was described initially as a sylvatic virus circulating between sloths (*Bradypus tridactylus*), monkeys (*Saguinus* spp., *Saimiri* spp., and *Alouatta belzebul*), and other animals, with only episodic outbreaks in humans (12), recent studies indicate that OROV circulates in urban areas of South America and was associated with approximately 2 to 6% of undifferentiated febrile patients in 13 locations in Ecuador, Peru, Bolivia (9, 13), and Brazil (14). Consistent with this observation, the seroprevalence for OROV in urban areas in the Amazon ranges between 15 and 33% (13, 15). Climate change, expansion and dissemination of arthropod vectors, and human travel increase the likelihood that OROV will emerge as a pathogen of greater significance in new areas. Several arthropod vectors contribute to OROV transmission, including *Culicoides paraensis* and *Culex quinquefasciatus* in the urban cycle and *Aedes serratus* and *Coquillettidia venezuelensis* in the sylvatic cycle. Other species of *Aedes* mosquitoes, including *Aedes albopictus*, can sustain OROV infection in laboratory settings (16).

In humans, OROV infection causes Oropouche fever, a severe febrile illness associated with headache, myalgia, arthralgia, malaise, and skin rash. Viremia is detected only during the first few days of infection. Hemorrhagic phenomena (petechiae, epistaxis, and gingival bleeding) have been reported in some patients (17). Although most patients with Oropouche fever recover within 2 to 3 weeks of initial infection without long-term sequelae (12), symptoms can persist for months and, surprisingly, relapses are common (12). In some patients, OROV infection progresses to meningitis and/or encephalitis (18–20). Indeed, OROV was detected in the cerebrospinal fluid of almost 7% of patients with meningoencephalitis who were suspected of having an acute viral infection of the central nervous system (CNS) in some settings (18, 19). Neurological signs and symptoms in patients with OROV fever include vertigo, lethargy, diplopia, nystagmus, and nuchal rigidity (12, 20).

Despite its potential for further geographical spread, little is known about OROV pathogenesis. In two animal models (adult golden hamster [*Mesocricetus auratus*] and neonatal BALB/c mice), OROV was detected in the brain and spinal cord, associated with pathological evidence of encephalitis, and resulted in lethality (30% of hamsters [21] and 85% of neonatal mice [22]). Recently, a study suggested that during the early phases of infection, OROV disseminates to the CNS via the spinal cord and subsequently transits to the brain, presumably through retrograde axonal transport (23). However, OROV has not been reported to replicate efficiently or cause disease in adult immunocompetent mice, and little is known about the host factors that restrict OROV infection in peripheral organs or in the CNS tissues of these animals.

Analogous to other arthropod-borne viruses (e.g., dengue [24] and chikungunya [25]), we hypothesized that the limited infection in adult mice might reflect restriction of OROV by innate immune host defense pathways in mature murine cells. The type I interferon (IFN) signaling network is essential for antiviral defense and has a pivotal role in age-dependent mortality in mice (25). This response is initiated by recognition of non-self pathogen-associated molecular patterns (PAMPs), including viral nucleic acids, and by host pattern recognition receptors (PRRs), including Toll-like receptors (TLR3 and TLR7) and RIG-I-like receptors (RLRs; RIG-I and MDA5) (26–29). TLRs and RLRs recognize distinct RNA PAMPs in the endosome and cytoplasm, respectively, and activate signaling cascades to initiate host defense responses. Both PRR pathways can induce nuclear localization of the transcription factors IRF-3, IRF-7, and NF-κB to induce the expression of type I IFN and proinflammatory cytokines (30). Type I IFN signaling induces an antiviral state by triggering expression of several hundred IFN-stimulated genes (ISGs), which block viral entry, replication, translation, and assembly as well as modulate inflammation and adaptive immunity (31).

Although little is known about how the innate immune system restricts OROV, type I IFN protects against related orthobunyaviruses (32), even though several genus members have mechanisms to inhibit type I IFN production by infected cells (33–35). Adult mice deficient in the type I IFN receptor (*Ifnar*$^{-/-}$) are more vulnerable to infection by La Crosse (LACV), Schmallenberg (SBV), and Bunyamwera (BUNV) viruses than wild-type (WT) mice (34, 36, 37). Members of the more distantly related *Phlebovirus* and *Nairovirus* genera, including Rift Valley fever virus (RVFV) and Crimean-Congo hemorrhagic fever virus (CCHFV), also are more pathogenic in *Ifnar*$^{-/-}$ mice (38, 39). IRF-3- and IRF-7-dependent transcription contributes to the control of LACV infection *in vivo* (40), as their combined deficiency resulted in more rapid death (40, 41). However, a deficiency of MAVS paradoxically resulted in an improved clinical outcome after LACV infection (40), suggesting that under certain circumstances MAVS-dependent signaling may cause neuronal pathogenesis *in vivo*.

To begin to define the role of PRRs and type I IFN induction and signaling pathways on OROV pathogenesis, we studied the morbidity, mortality, tissue tropism, and cytokine responses from OROV-infected mice with targeted gene deletions in IFNAR, IFN-β, MDA5, MAVS, IRF-3, and IRF-7. In parallel, we analyzed the kinetics of OROV infection *ex vivo* in primary fibroblasts (MEFs), macrophages (Mϕ), and dendritic cells (DCs). Our experiments show a prominent protective role for MAVS, IRF-3 and IRF-7, and IFNAR in restricting OROV infection and tissue injury and establish that type I IFN signaling in nonmyeloid cells likely contributes to the antiviral response against orthobunyaviruses.

MATERIALS AND METHODS

Viruses and cells. The OROV strain (Bean 19991) was provided by Eurico Arruda (Ribeirão Preto, Brazil) and passaged three times in Vero cells to produce the virus stock. This stock was clarified by centrifugation (5,000 × *g* for 5 min) and stored at −80°C. The titer of the stock virus was determined by focus-forming assay and calculated as 2.0×10^7 focus-forming units (FFU) per ml. All experiments with OROV were conducted under enhanced biosafety level 3 (BSL3) and animal (A)-BSL3 containment at Washington University with the appropriate personal protective equipment and approval from the United States Department of Agriculture. The LACV strain (original strain) was provided generously by Andrew Pekosz (Johns Hopkins University, Baltimore, MD, USA) and passaged twice in Vero cells to produce a virus stock. This stock was clarified and stored at −80°C. The titer of LACV was calculated as 2.7×10^7 FFU/ml using the monoclonal antibodies (MAb; 807-31 and 807-33) that also were provided by Andrew Pekosz (42, 43). Experiments with LACV were conducted in BSL2 and A-BSL3 facilities.

Ethics statement. This study was carried out in strict accordance with the recommendations in the *Guide for the Care and Use of Laboratory Animals* of the National Institutes of Health (44) after approval by the Institutional Animal Care and Use Committee at the Washington University School of Medicine (assurance number A3381-01). All injections with virus were performed under anesthesia with ketamine hydrochloride (80 mg/kg of body weight) and xylazine (15 mg/kg).

Mouse experiments. All mice were on a C57BL/6 background. WT mice (CD45.1 and CD45.2) were purchased from Jackson Laboratories and/or bred in a specific-pathogen-free facility at Washington University. *Ifnar*$^{-/-}$, *Ifnb*$^{-/-}$, *Mda5*$^{-/-}$, *Mavs*$^{-/-}$, *Irf3*$^{-/-}$, *Irf7*$^{-/-}$, and *Irf3*$^{-/-}$ × *Irf7*$^{-/-}$ (double-knockout [DKO]) mice were described previously (45–50). CD11c Cre^{+} *Ifnar*$^{f/f}$, LysM Cre^{+} *Ifnar*$^{f/f}$, and Cre^{-} *Ifnar*$^{f/f}$ mice also were described previously (51). All infections were performed by subcutaneous injection in the footpad with 10^6 FFU of OROV and 10^5 or 10^6 FFU of LACV in a volume of 50 μl using 5- to 6-week-old mice. All animals were monitored for survival and weight loss for 21 days.

Bone marrow chimera and transfers. Bone marrow cells were collected from adult C57BL/6 WT (CD45.1) or *Ifnar*$^{-/-}$ (CD45.2) mice and transferred adoptively (10^7 cells per animal) by retroorbital injection into 4-week-old 800-cGy-irradiated WT (CD45.1 or CD45.2) or *Ifnar*$^{-/-}$ mice. Eight weeks later, reconstitution was validated by flow cytometry and mice were infected with OROV. Four days later, serum and tissues were harvested for blood chemistry and viral titer analyses.

Tissue harvest and virus titration. OROV-infected mice were sacrificed on days 1, 2, 4, or 6 postinfection. After perfusion (20 ml) with phosphate-buffered saline (PBS), organs (liver, spleen, kidney, lung, heart, brain, and spinal cord) were harvested, weighed, homogenized using zirconia beads in a MagNA Lyser instrument (Roche Life Science) in 1 ml of minimal essential medium (MEM) with 2% heat-inactivated fetal bovine serum (FBS), and stored at −80°C until virus titration. Approximately 200 μl of serum from all infected animals was collected and stored at −80°C.

For OROV titration, samples were thawed, clarified by centrifugation (2,000 × *g* at 4°C for 10 min), and diluted serially prior to infection of Vero cells in 96-well plates. After 22 to 24 h of infection, the cells were fixed overnight with 1% paraformaldehyde (PFA) in PBS. Infected cell foci were detected after incubation with a 1:1,000 dilution of polyclonal mouse anti-OROV ascites fluid (ATCC VR-1228AF) in a volume of 50 μl for 2 h at room temperature. After three washes with 300 μl of permeabilization-wash buffer (P-W; PBS, 0.1% saponin, and 0.1% bovine serum albumin [BSA]), the samples were incubated with 50 μl of a 1:2,000 dilution of horseradish peroxidase (HRP)-conjugated goat anti-mouse IgG (Sigma) for 1 h at room temperature. After three additional washes with P-W, staining was visualized by the addition of the TrueBlue detection reagent (KPL), and the spots were analyzed after three washes with 300 μl of distilled water with a Biospot counter (Cellular Technology) using Immunocapture software. All results were converted into FFU per gram of tissue, with the exception of serum samples, which were expressed as FFU per milliliter of serum.

Blood chemistry analysis. On day 4 or 6 after OROV infection of WT, *Ifnar*$^{-/-}$, *Mavs*$^{-/-}$, or *Irf3*$^{-/-}$ × *Irf7*$^{-/-}$ DKO mice, blood was collected by intracardiac puncture and serum was isolated. Samples were treated with β-propiolactone (BPL; Sigma Chemical) for 30 min at 37°C to inactivate infectious virus. Blood chemistry analyses were performed using a Catalyst Dx chemistry analyzer (IDEX Laboratories). Control experiments confirmed that BPL treatment of OROV did not impact chemistry results (data not shown).

Histology, immunohistochemistry, and TUNEL staining. Mice from each group (WT, *Ifnar*$^{-/-}$, *Mavs*$^{-/-}$, and *Irf3*$^{-/-}$ × *Irf7*$^{-/-}$ DKO) were infected with OROV, and 4 days later liver and spleen were harvested, fixed in 4% PFA in PBS for 24 h at 4°C, dehydrated in increasing ethanol concentrations, and paraffin embedded. Hematoxylin and eosin staining and terminal deoxynucleotidyltransferase-mediated dUTP-biotin nick end labeling (TUNEL) staining of paraffin-embedded tissues were performed by the Digestive Diseases Research Core Center of Washington University. TUNEL staining was performed using a POD *in situ* cell death detection kit (Roche) as described by the manufacturer.

Detection of OROV antigen was performed on 5-μm paraffin tissue sections. Sections were deparaffinized, rehydrated, and treated for antigen retrieval in Tris-borate buffer (pH 7.6) supplemented with 0.05% of a protease enzyme derived from *Streptomyces griseus* (Sigma), followed by incubation with 0.6% H_2O_2 in methanol for 30 min to block the activity of endogenous peroxidases. Sections were then blocked for avidin and biotin with a commercial kit (DakoCytomation biotin blocking system). Subsequently, the "Mouse on Mouse" (M.O.M.) immunodetection kit was used according to the manufacturer's protocol (Vector Laboratories). The sections were incubated sequentially with M.O.M. mouse immunoglobulin-blocking reagent and mouse polyclonal anti-OROV or control ascites fluid (1:100) for 30 min. The binding of primary antibody was detected using M.O.M. biotinylated anti-mouse IgG antibody and a 1:300 dilution of streptavidin-peroxidase ultrasensitive polymer (Sigma). Antigen staining was visualized using DAB (3,3′-diaminobenzidine) HRP substrate (Vector) and then counterstained with hematoxylin. Tissue sections were visualized at 20× and 40× magnification using a Zeiss Axioskop 40 microscope attached to an AxioCam MRc digital color camera.

Cytokine Bio-Plex assay. On days 4 and 6 after OROV infection of WT, *Ifnar*$^{-/-}$, *Mavs*$^{-/-}$, and *Irf3*$^{-/-}$ × *Irf7*$^{-/-}$ DKO mice, serum was collected and cytokine levels were analyzed using the Bio-Plex Pro mouse cytokine assay (Bio-Rad). This platform includes the following cytokines and chemokines: interleukin 1α (IL-1α), IL-1β, IL-2, IL-3, IL-4, IL-6, IL-9, IL-10, IL-12p40, IL-12p70, IL-13, IL-17, eotaxin (CCL11), granulocyte colony-stimulating factor (G-CSF), granulocyte-macrophage colony-stimulating factor (GM-CSF), IFN-γ, KC (CXCL1), monocyte chemoattractant protein 1 (MCP-1) (CCL-2), MIP-1α (CCL3), MIP-1β (CCL4), RANTES (CCL5), and tumor necrosis factor alpha (TNF-α).

OROV replication in primary mouse cells. Primary mouse fibroblasts (MEFs) from WT, *Ifnar*$^{-/-}$, *Mavs*$^{-/-}$, *Mda5*$^{-/-}$, or *Irf3*$^{-/-}$ × *Irf7*$^{-/-}$ DKO mice were generated as described previously (47). MEFs from *Rig-I*$^{-/-}$ mice and their WT controls were a gift from Michael Gale (Seattle, WA). Mϕ and DC cultures were produced as described previously (52). Bone marrow was isolated from mice and cultured for 7 days in medium supplemented with 40 ng/ml M-CSF (PeproTech) or 20 ng/ml of both GM-CSF and IL-4 (PeproTech) to produce Mϕ and DCs, respectively. Multistep virus growth curves were performed at a multiplicity of infection (MOI) of 0.001. The viral titer in the cell-free supernatant was determined by FFU assay on Vero cells at the following time points after infection: 0, 1, 4, 12, 24, 36, 48, and 60 h.

Quantification of type I IFN and IFN-stimulated genes (ISGs) in murine cells. The levels of type I IFN and *Ifit1* mRNA were determined by quantitative reverse transcription-PCR (qRT-PCR). WT, *Ifnar*$^{-/-}$, *Mavs*$^{-/-}$, or *Irf3*$^{-/-}$ × *Irf7*$^{-/-}$ DKO MEFs were infected with OROV at an MOI of 0.1. Cells were harvested at 1, 4, 12, 24, and 36 h after infection, and the total RNA was extracted using the RNeasy kit (Qiagen) and treated with TURBO DNase (Life Technologies) for 2 h at 37°C. qRT-PCR for *Ifna*, *Ifnb*, *Ifit1*, and *Gapdh* mRNA was performed by using one-step qRT-PCR master mix, with the indicated primers and probes (Table 1). One-step qRT-PCR also confirmed OROV infection in these cells (data not shown) by using the indicated primers and probes (Table 1). All reactions were assembled in a final volume of 25 μl with 300 ng of RNA, 1× PrimeTime mix (Integrated DNA Technologies) containing both primers and probe, and 12.5 μl of TaqMan master mix (Applied Biosystems) by using the following cycling algorithm: 48°C for 30 min, 95°C for 10 min, followed by 45 cycles of 95°C for 15 s and 60°C for 1 min. All reactions were normalized to 18S RNA levels by using the eukaryotic 18S rRNA endogenous control kit (Applied Biosystems) and expressed on a $\log_2$ scale as fold increase over mock (same time point in a noninfected MEF culture) according to the threshold cycle ($\Delta\Delta C_T$) method (53).

The levels of secreted IFN-β protein in supernatants of OROV-in-

TABLE 1 Primers and probes used for qRT-PCR

Target[a]	Sequence[b]	Reference
OROV		83
Fwd	5′-TACCCAGATGCGATCACCAA-3′	
Rev	5′-TTGCGTCACCATCATTCCAA-3′	
Probe	5′-56-FAM-TGCCTTTGGCTGAGGTAAAGGGCTG-36-TAMSp-3′	
Mouse *Gapdh*		84
Fwd	5′-AATGGTGAAGGTCGGTGTG-3′	
Rev	5′-GTGGAGTCATACTGGAACATGTAG-3′	
Probe	5′-56-FAM-TGCAAATGG-ZEN-CAGCCCTGGTG-3IABkFQ-3′	
Mouse *Ifna*		84
Fwd	5′-CTTCCACAGGATCACTGTGTACCT-3′	
Rev	5′-TTCTGCTCTGACCACCTCCC-3′	
Probe	5′-56-FAM-AGAGAGAAGAAACACAGCCCCTGTGCC-36-TAMSp-3′	
Mouse *Ifnb*		52
Fwd	5′-GGCTTCCATCATGAACAACAG-3′	
Rev	5′-GTTGATGGAGAGGGCTGTG-3′	
Probe	5′-56-FAM-CTGCGTTCCTGCTGTGCTTCTC-36-TAMSp-3′	
Mouse *Ifit1*		52
Fwd	5′-GAGCCAGAAAACCCTGAGTACA-3′	
Rev	5′-AGAAATAAAGTTGTCATCTAAATC-3′	
Probe	5′-56-FAM-ACTGGCTATGCAGTCGTAGCCTATCGCC-36-TAMSp-3′	

[a] Fwd, forward; Rev, reverse.
[b] FAM, 6-carboxyfluorescein; TAMsp, 6-carboxytetramethylrhodamine; ZEN, double-quenched probe; 3IABkFQ, 3′ Iowa Black FQ.

fected MEFs were measured by a commercial capture enzyme-linked immunosorbent assay (ELISA) kit (PBL Laboratories).

OROV replication in U3A and 2fTGH human cells and quantification of type I IFN and ISGs. Virus replication and type I IFN mRNA production were determined by qRT-PCR in 2fTGH-infected (fibrosarcoma cells) and U3A-infected (2fTGH-derived STAT1-deficient mutant cells) cells at an MOI of 0.1. Cells were harvested at 1, 4, 12, 24, and 36 h after infection, and total RNA was obtained as described in the previous section. The levels of viral RNA were measured by qRT-PCR as described above and expressed on a $\log_{10}$ scale as genome equivalents/sample after comparison with a standard curve produced using serial 10-fold dilutions of OROV RNA. The levels of human *IFNB*, *IFIT1*, and *GAPDH* mRNA were determined after normalization to 18S levels and expressed on a $\log_2$ scale as fold increase over mock, as described in the previous section. All primers and probes were obtained from Integrated DNA Technologies (PrimeTime catalogue number for *IFNB*, Hs.PT.58.39481063.g, for *IFIT1*, Hs.PT.56a.20769090.g, and for *GAPDH*, Hs.PT.39a.22214836).

Statistical analysis. All data were analyzed using Prism software (GraphPad Software). Kaplan-Meier survival curves were analyzed by the log rank test, and weight loss values at a given time point were compared using 2-way analysis of variance (ANOVA). For viral burden analysis, the log titers were analyzed by the Mann-Whitney test. Type I IFN levels and qRT-PCR also were compared using 2-way ANOVA. A P value of <0.05 indicated statistically significant differences relative to the indicated control group.

RESULTS

***Ifnar*$^{-/-}$, *Mavs*$^{-/-}$, and *Irf3*$^{-/-}$ × *Irf7*$^{-/-}$ DKO mice are vulnerable to lethal OROV infection.** Similar to other orthobunyaviruses, in mice, OROV virulence is age dependent, with older animals more resistant to lethal infection (22). Injection of 10^6 FFU of OROV by a subcutaneous route induced uniformly lethal disease in newborn C57BL/6 WT mice. Three-day-old mice infected with OROV exhibited 66.6% mortality, whereas 3-, 5-, or 9-week-old mice did not succumb to infection (data not shown).

Because studies with other arthropod-borne viruses have shown that age-dependent mortality is determined in part by changes in innate immune responses (25), we hypothesized that young adult C57BL/6 mice, which normally are resistant to lethal OROV infection, might become sensitive if key proteins in the type I IFN induction and/or signaling pathway were absent. Accordingly, we evaluated OROV pathogenesis in 6-week-old *Ifnar*$^{-/-}$, *Ifnb*$^{-/-}$, *Mda5*$^{-/-}$, *Mavs*$^{-/-}$, *Irf3*$^{-/-}$, *Irf7*$^{-/-}$, and *Irf3*$^{-/-}$ × *Irf7*$^{-/-}$ DKO mice. OROV infection of 6-week-old *Ifnar*$^{-/-}$ mice, which cannot respond to type I IFN, resulted in 100% mortality, with a mean survival time of 5 days and significant weight loss (Fig. 1A and C). In contrast, 6-week-old WT mice did not show disease signs or weight loss compared to uninfected animals (Fig. 1B). OROV-infected *Ifnar*$^{-/-}$ mice exhibited lethargy and decreased body temperature, especially late in the course of disease (data not shown). However, signs of neuroinvasive disease, including limb paralysis, ataxia, seizures, or sustained tremors, were not apparent in OROV-infected *Ifnar*$^{-/-}$ mice. A protective role for IFN-β was supported by studies with 6-week-old *Ifnb*$^{-/-}$ mice infected with OROV (Fig. 1A). Although only a relatively small increase in lethality (17%) was observed in *Ifnb*$^{-/-}$ mice, this attained statistical significance ($P < 0.02$); this phenotype corresponded with greater weight loss in *Ifnb*$^{-/-}$ animals that survived OROV challenge or succumbed to lethal infection (Fig. 1F) than in WT mice. Given this difference in disease severity between *Ifnar*$^{-/-}$ and *Ifnb*$^{-/-}$ mice after OROV infection, it is likely that other type I IFNs (e.g., IFN-α) restrict OROV in adult mice.

To determine whether the RLR signaling pathway contributed to host recognition of OROV and induction of antiviral responses, we infected 6-week-old *Mda5*$^{-/-}$ and *Mavs*$^{-/-}$ mice. *Mda5*$^{-/-}$ mice did not succumb to OROV infection (Fig. 1A) or show any

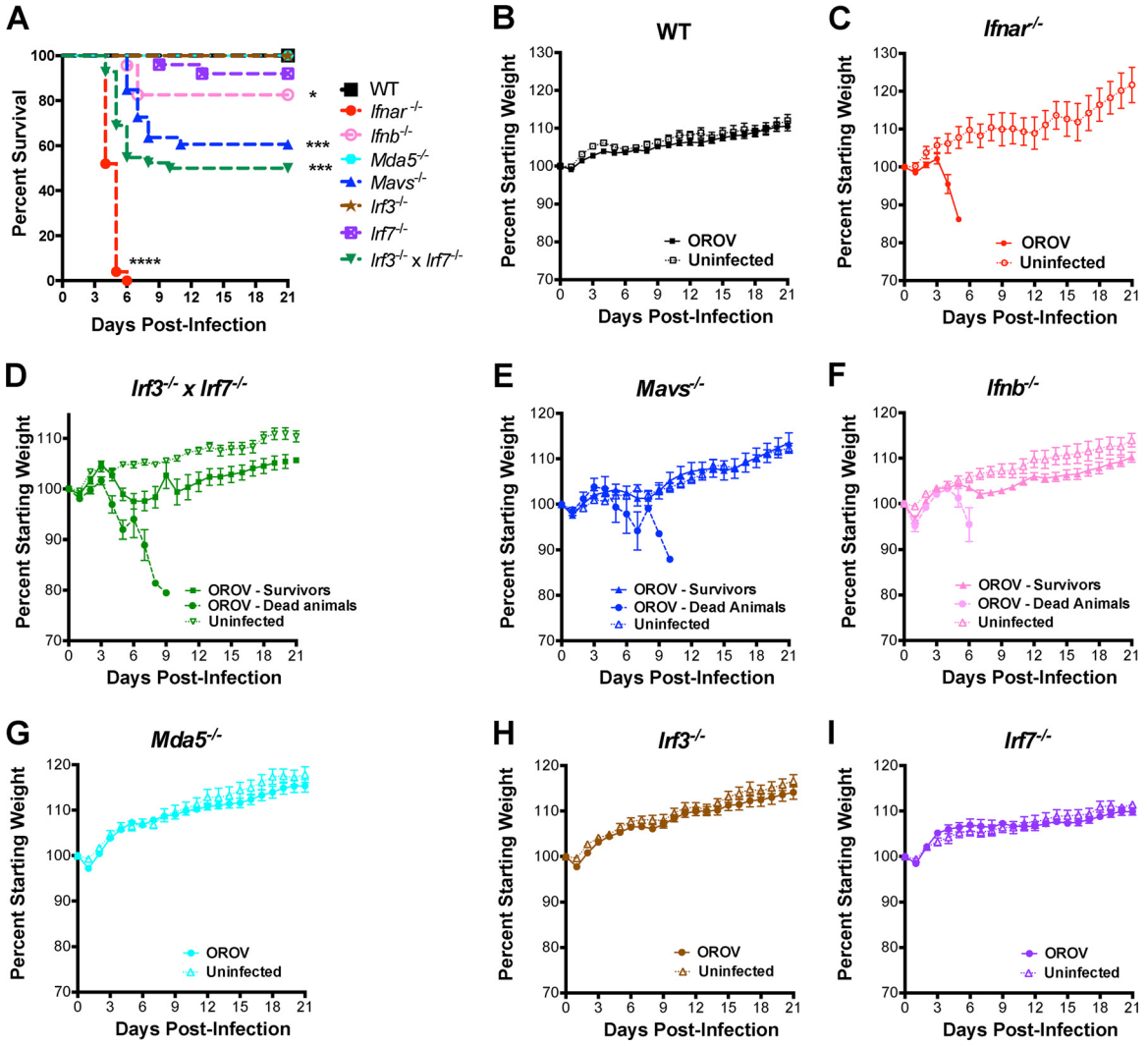

FIG 1 Mice with targeted deletions in the IFN induction or signaling pathway are more vulnerable to OROV infection. (A) Survival analysis of 6-week-old mice after inoculation with 10^6 PFU of OROV by subcutaneous injection in the footpad: WT ($n = 33$), *Ifnar*$^{-/-}$ ($n = 25$), *Ifnb*$^{-/-}$ ($n = 23$), *Mda5*$^{-/-}$ ($n = 24$), *Mavs*$^{-/-}$ ($n = 33$), *Irf3*$^{-/-}$ ($n = 40$), *Irf7*$^{-/-}$ ($n = 25$), and *Irf3*$^{-/-}$ × *Irf7*$^{-/-}$ DKO ($n = 39$) mice were used for survival curves. Data are pooled from at least three independent experiments. Asterisks indicate differences that were statistically significant compared to WT mice by the log rank test (**, $P < 0.01$; ***, $P < 0.001$). (B to I) Weight loss in infected (dead or surviving animals considered separately) and uninfected mice in WT ($n = 33$ and $n = 10$ for infected and uninfected mice, respectively) (B), *Ifnar*$^{-/-}$ ($n = 25$ infected and $n = 3$ uninfected) (C), *Irf3*$^{-/-}$ × *Irf 7*$^{-/-}$ DKO ($n = 14$ dead, $n = 19$ survivors, and $n = 13$ uninfected) (D), *Mavs*$^{-/-}$ ($n = 13$ dead, $n = 20$ survivors, and $n = 10$ uninfected) (E), *Ifnb*$^{-/-}$ ($n = 4$ dead, $n = 19$ survivors, and $n = 8$ uninfected) (F), *Mda5*$^{-/-}$ ($n = 24$ infected and $n = 8$ uninfected) (G), *Irf3*$^{-/-}$ ($n = 40$ infected and $n = 15$ uninfected) (H), and *Irf7*$^{-/-}$ ($n = 25$ infected and $n = 9$ uninfected) (I) mice. The weight loss curves were compared using 2-way ANOVA.

disease signs or weight loss compared to WT mice (Fig. 1G). In comparison, *Mavs*$^{-/-}$ mice were vulnerable to OROV infection, with a mortality rate of 39% (Fig. 1A), although weight loss differences were not observed in the surviving animals (Fig. 1E). These results indicate that RLR recognition of OROV contributes to the host defense response *in vivo*, likely with a dominant effect of RIG-I. However, we were unable to test OROV infection in *Rig-I*$^{-/-}$ mice, as a Rig-I deficiency on a congenic C57BL/6 background is embryonic lethal (54).

To assess the impact of the transcription factors downstream of RLR signaling and upstream of IFN-α and IFN-β induction, we infected *Irf3*$^{-/-}$, *Irf7*$^{-/-}$, or *Irf3*$^{-/-}$ × *Irf7*$^{-/-}$ DKO mice with OROV. Whereas *Irf3*$^{-/-}$ or *Irf7*$^{-/-}$ single-KO mice showed no enhanced mortality (Fig. 1A) or weight loss (Fig. 1H and I) after OROV inoculation, 54% of *Irf3*$^{-/-}$ × *Irf7*$^{-/-}$ DKO mice succumbed to infection (Fig. 1A), and the surviving animals gained weight more slowly than uninfected mice (Fig. 1D). Collectively, these survival and morbidity studies suggest that RLR-mediated detection (likely RIG-I), MAVS signaling, IRF-3 and IRF-7 transcriptional activity, and type I IFN responses are important components of the protective antiviral response against OROV in adult mice.

OROV replicates preferentially in the liver, spleen, and blood of mice lacking intact type I IFN signaling. To assess how type I IFN signaling impacts OROV tropism and replication in 6-week-old mice, we measured viral burden in the serum, liver, spleen, kidney, lung, heart, brain, and spinal cord on days 1, 2, 4, and 6 after infection of WT, *Ifnar*$^{-/-}$, *Mavs*$^{-/-}$, and *Irf3*$^{-/-}$ × *Irf7*$^{-/-}$

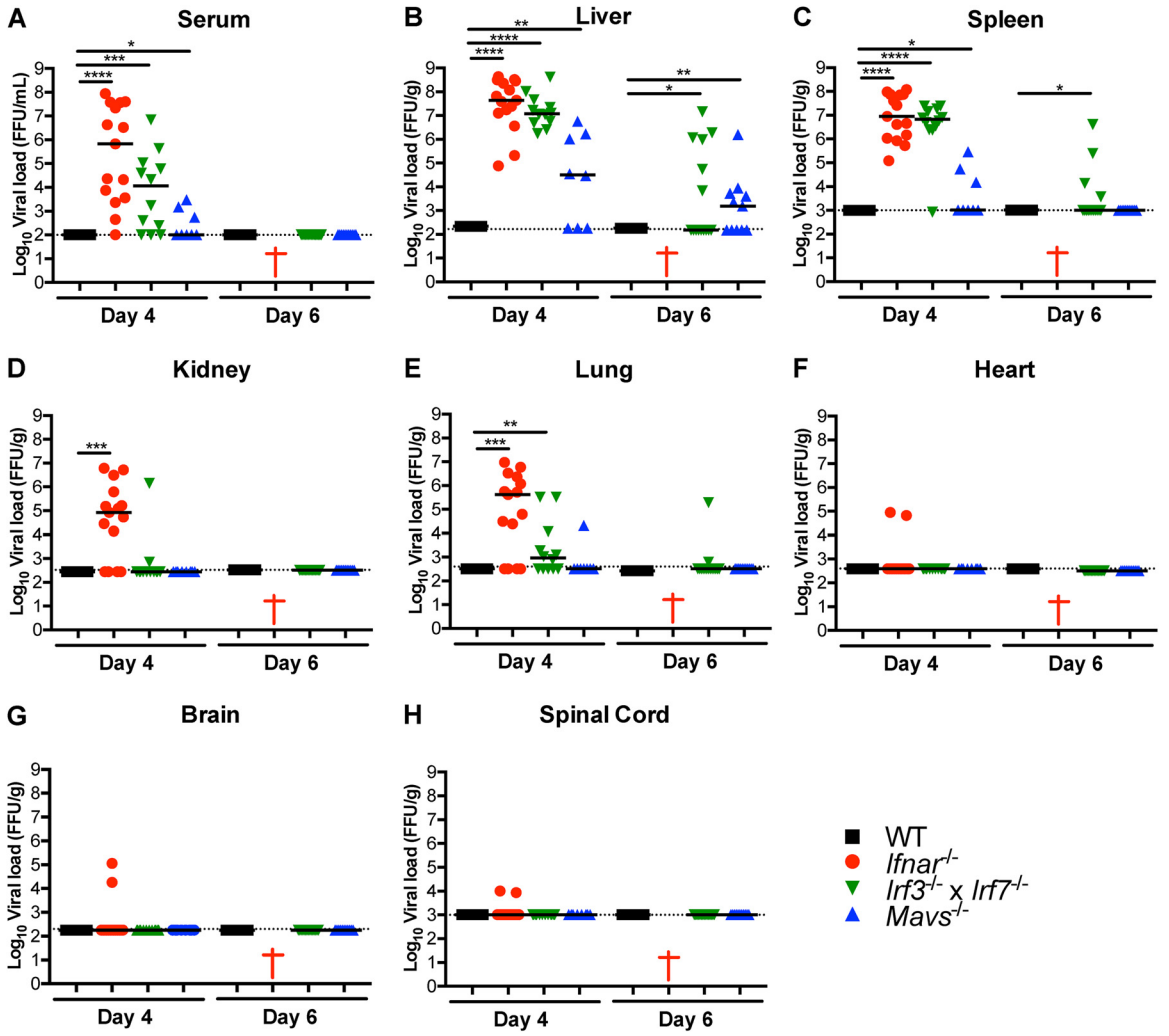

FIG 2 Tissue viral burden in *Ifnar*$^{-/-}$, *Mavs*$^{-/-}$, and *Irf3*$^{-/-}$ × *Irf7*$^{-/-}$ DKO mice infected with OROV. Viral burden after OROV infection of *Ifnar*$^{-/-}$, *Mavs*$^{-/-}$, and *Irf3*$^{-/-}$ × *Irf7*$^{-/-}$ DKO mice was measured by focus-forming assay in samples from serum (A), liver (B), spleen (C), kidney (D), lung (E), heart (F), brain (G), and spinal cord (H). Data points represent individual mice. Bars indicate median values and were obtained from 8 to 15 mice per time point. Dashed lines represent the limit of sensitivity of the assay. Asterisks indicate statistical significance as judged by the Mann-Whitney test (*, $P < 0.05$; **, $P < 0.01$; ***, $P < 0.001$; ****, $P < 0.0001$). The red cross indicates that all OROV-infected *Ifnar*$^{-/-}$ animals were dead at the indicated time point.

DKO mice. On day 1 after infection, we did not detect infectious virus in any tissue from the different genotypes. We detected virus as early as day 2 after infection in the liver and serum of *Ifnar*$^{-/-}$ mice but not in other tissue samples. In comparison, by day 4 after infection, high levels (1.2×10^5 to 4.3×10^8 FFU/g) of OROV were recovered from the liver and spleen of all *Ifnar*$^{-/-}$ and *Irf3*$^{-/-}$ × *Irf7*$^{-/-}$ DKO mice (Fig. 2A and B). Lower (2.5×10^2 to 4.1×10^7 FFU/ml or FFU/g) yet significant levels of OROV also were measured in the serum, kidneys, and lungs of *Ifnar*$^{-/-}$ and *Irf3*$^{-/-}$ × *Irf7*$^{-/-}$ DKO mice on day 4 after infection (Fig. 2C to E). OROV was detected in the heart, brain, and spinal cord in only 2 of 15 *Ifnar*$^{-/-}$ mice (Fig. 2F to H). Infectious OROV was present in ~50% of the *Irf3*$^{-/-}$ × *Irf7*$^{-/-}$ DKO mice in the liver and spleen at day 6 after infection (3.7×10^3 to 1.5×10^7 FFU/g).

In comparison to *Ifnar*$^{-/-}$ or *Irf3*$^{-/-}$ × *Irf7*$^{-/-}$ DKO mice, infectious OROV was detected in only a subset of tissues samples from *Mavs*$^{-/-}$ mice, including the liver and spleen on day 4 after infection. The viral titers in *Mavs*$^{-/-}$ mice generally were lower (1.5×10^4 to 5.7×10^6 FFU/g) (Fig. 2A to H) and cleared by day 6 after infection in the spleen, lung, and serum. In contrast, in the liver, OROV was present in 6 of 11 *Mavs*$^{-/-}$ mice (4×10^3 to 1.6×10^6 FFU/g) on day 6. These data suggest that other pathogen recognition and signaling pathways (e.g., TLR and MyD88) likely contribute to the induction of type I IFN responses and restriction of OROV in specific tissues.

Blood chemistry reveals extensive liver injury. To understand the basis for disease in the different KO mice after OROV infection, we analyzed their blood chemistries. On day 4 after infection, we observed significant liver injury in *Ifnar*$^{-/-}$, *Mavs*$^{-/-}$, and *Irf3*$^{-/-}$ × *Irf7*$^{-/-}$ DKO mice, as reflected by increased levels of alanine aminotransferase (ALT) (7,307 U/liter, 601 U/liter, and 7,164 U/liter, respectively, compared to 111 U/liter in infected WT mice; $P < 0.01$) (Fig. 3A) and aspartate aminotransferase (AST) (8,387 U/liter, 827 U/liter, and 7,438 U/liter, respectively, compared to 372 U/liter in infected WT mice; $P < 0.01$) (Fig. 3B). Liver damage also was suggested by the relative

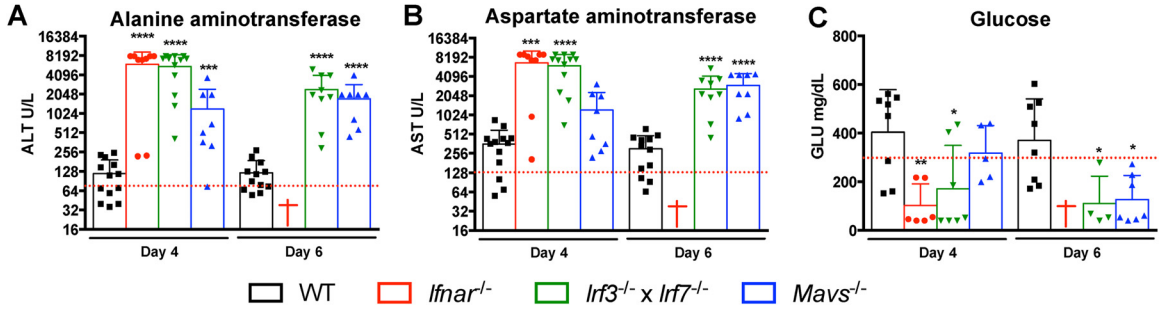

FIG 3 Blood chemistry reveals extensive liver injury after OROV infection. Alanine aminotransferase (ALT) (A), aspartate aminotransferase (AST) (B), and glucose (GLU) (C) levels were measured from serum samples of WT and *Ifnar*$^{-/-}$, *Mavs*$^{-/-}$, and *Irf3*$^{-/-}$ × *Irf7*$^{-/-}$ mice ($n = 8$ to 13 for each group) obtained 4 and 6 days after infection with 10^6 FFU of OROV. Data points represent individual mice and are pooled from three independent experiments. Asterisks indicate statistical significance as judged by the Mann-Whitney test (*, $P < 0.05$; **, $P < 0.01$; ***, $P < 0.001$; ****, $P < 0.0001$). The red dotted lines represent the mean values from three mock-infected naive mice. In the mouse phenome database (Jackson Laboratory), the mean ALT, AST, and GLU levels in serum of 6- to 8-week-old C57BL/6J mice were 23.6 (±7.6), 94.0 (±48.9), and 176 (±31.4), respectively. A red cross indicates that all OROV-infected *Ifnar*$^{-/-}$ animals were dead at the indicated time point.

hypoglycemia in *Ifnar*$^{-/-}$, *Mavs*$^{-/-}$, and *Irf3*$^{-/-}$ × *Irf7*$^{-/-}$ DKO mice (glucose [GLU] levels of 50.5 mg/dl, 295.0 mg/dl, and 52.0 mg/dl, respectively) compared to in infected WT mice (494.0 mg/dl; $P < 0.05$) (Fig. 3C). In comparison, serum levels of blood urea nitrogen, creatinine, alkaline phosphatase, and creatine kinase were similar between infected WT and KO animals (data not shown). The levels of AST and ALT remained high on day 6 after infection in the surviving KO mice (Fig. 3B) and reflect acute hepatic injury, which may be due to direct virus-induced lysis of hepatocytes, immune-mediated injury, or ischemia.

Pathological and immunohistochemical analysis of the liver and spleen from OROV-infected mice. To define the basis for the tissue damage associated with OROV infection, we performed pathological analysis on liver and spleen isolated from WT *Ifnar*$^{-/-}$, *Mavs*$^{-/-}$, and *Irf3*$^{-/-}$ × *Irf7*$^{-/-}$ DKO mice on days 4 and 6 after infection. Necropsy revealed gross macroscopic tissue damage in the liver of *Ifnar*$^{-/-}$ and *Irf3*$^{-/-}$ × *Irf7*$^{-/-}$ DKO mice, which was characterized by visible hemorrhages and tissue discoloration in several animals (data not shown). Hematoxylin and eosin staining of paraffin sections revealed areas of focal cellular necrosis within the liver of *Ifnar*$^{-/-}$ and *Irf3*$^{-/-}$ × *Irf7*$^{-/-}$ DKO but not in *Mavs*$^{-/-}$ or WT mice by day 4 after OROV infection (Fig. 4A and B; data not shown); this result correlated with the higher serum levels of liver enzymes (AST and ALT) in *Ifnar*$^{-/-}$ and *Irf3*$^{-/-}$ × *Irf7*$^{-/-}$ DKO mice than in WT mice at this time point (see Fig. 3A and B). By day 6 after OROV infection, tissue injury in the liver became apparent in *Mavs*$^{-/-}$ mice (data not shown). TUNEL staining showed a greater number of dead cells in the liver and spleen of *Ifnar*$^{-/-}$ and *Irf3*$^{-/-}$ × *Irf7*$^{-/-}$ DKO mice than in WT mice (Fig. 4C and D). Clusters of TUNEL-positive nuclei were present in the white and red pulp of the spleen (Fig. 4D) in all sections from OROV-infected *Ifnar*$^{-/-}$ and *Irf3*$^{-/-}$ × *Irf7*$^{-/-}$ DKO mice. Immunohistochemistry (IHC) was performed to determine if tissue damage correlated with viral infection. OROV antigen-positive cells were apparent on day 4 after infection in the liver of *Ifnar*$^{-/-}$ and *Irf3*$^{-/-}$ × *Irf7*$^{-/-}$ DKO but not WT mice (Fig. 4E). Small foci of OROV antigen-positive cells also were detected in the liver of *Mavs*$^{-/-}$ mice on day 6 after infection (data not shown). Based on cellular morphology and viral antigen staining, hepatocytes appear to be a major target of OROV infection. In contrast, in the spleen, OROV antigen-positive cells were observed only in sections of *Ifnar*$^{-/-}$ mice, in both the white and red pulp (Fig. 4F).

Hypercytokinemia in OROV-infected mice. To define additional possible mechanisms of tissue injury, we measured serum levels of 23 pro- and anti-inflammatory cytokines and chemokines on days 4 and 6 after OROV infection using Bio-Plex assays (Fig. 5 and Table 2). Although we did not observe elevated levels of inflammasome-generated (e.g., IL-1β) or vasoactive (e.g., TNF-α) cytokines in the infected KO mice, a marked increase in several proinflammatory cytokines (IL-6, IL-12p40, and G-CSF) on day 4 (*Ifnar*$^{-/-}$ and *Irf3*$^{-/-}$ × *Irf7*$^{-/-}$ DKO) and day 6 (*Mavs*$^{-/-}$) after OROV infection was apparent (Fig. 5A to C). The increased levels of these proinflammatory cytokines (e.g., IL-6) suggested a mechanism of production that was independent of MAVS, which contrasts with prior studies with flaviviruses (51). In comparison, the levels of IL-2, IL-3, IL-5, IL-10, IL-13, and IL-17A were not increased in the KO animals after OROV infection. However, higher levels of several (e.g., MCP-1, MIP-1α, KC, and RANTES) but not all (eotaxin and MIP-1β) chemokines were observed in OROV-infected KO mice than in WT mice (Fig. 5E to H and Table 2). Although some cytokine and chemokine levels were elevated in KO mice after OROV infection, the relatively minor change in IL-1β and TNF-α levels, coupled with the absence of renal damage, suggests that the disease pathogenesis occurs independently of a generalized cytokine storm.

OROV replication is enhanced in primary cell cultures with defects in IFN induction or signaling. To begin to determine how the components of the type I IFN induction and signaling pathway affected OROV infection in specific cell types, we performed multistep growth analysis in MEFs, DCs, and Mϕ derived from WT mice and *Mda5*$^{-/-}$, *Rig-I*$^{-/-}$, *Ifnar*$^{-/-}$, *Mavs*$^{-/-}$, and *Irf3*$^{-/-}$ × *Irf7*$^{-/-}$ DKO mice. In MEFs, deletion of either RIG-I or MDA-5 did not affect OROV infection substantively compared to titers observed in WT cells (Fig. 6A). However, OROV replicated to higher levels (2.3- to 4.2-fold, $P < 0.05$) in *Ifnar*$^{-/-}$, *Mavs*$^{-/-}$, and *Irf3*$^{-/-}$ × *Irf7*$^{-/-}$ DKO MEFs than in WT MEFs at 24 and 60 h after infection (Fig. 6B). In comparison, OROV replication was observed in bone marrow-derived DCs from *Ifnar*$^{-/-}$, *Mavs*$^{-/-}$, and *Irf3*$^{-/-}$ × *Irf7*$^{-/-}$ DKO mice but not from WT mice (Fig. 6C). For Mϕ, productive OROV infection was apparent only in cells derived from *Ifnar*$^{-/-}$ mice (Fig. 6D). These results suggest that

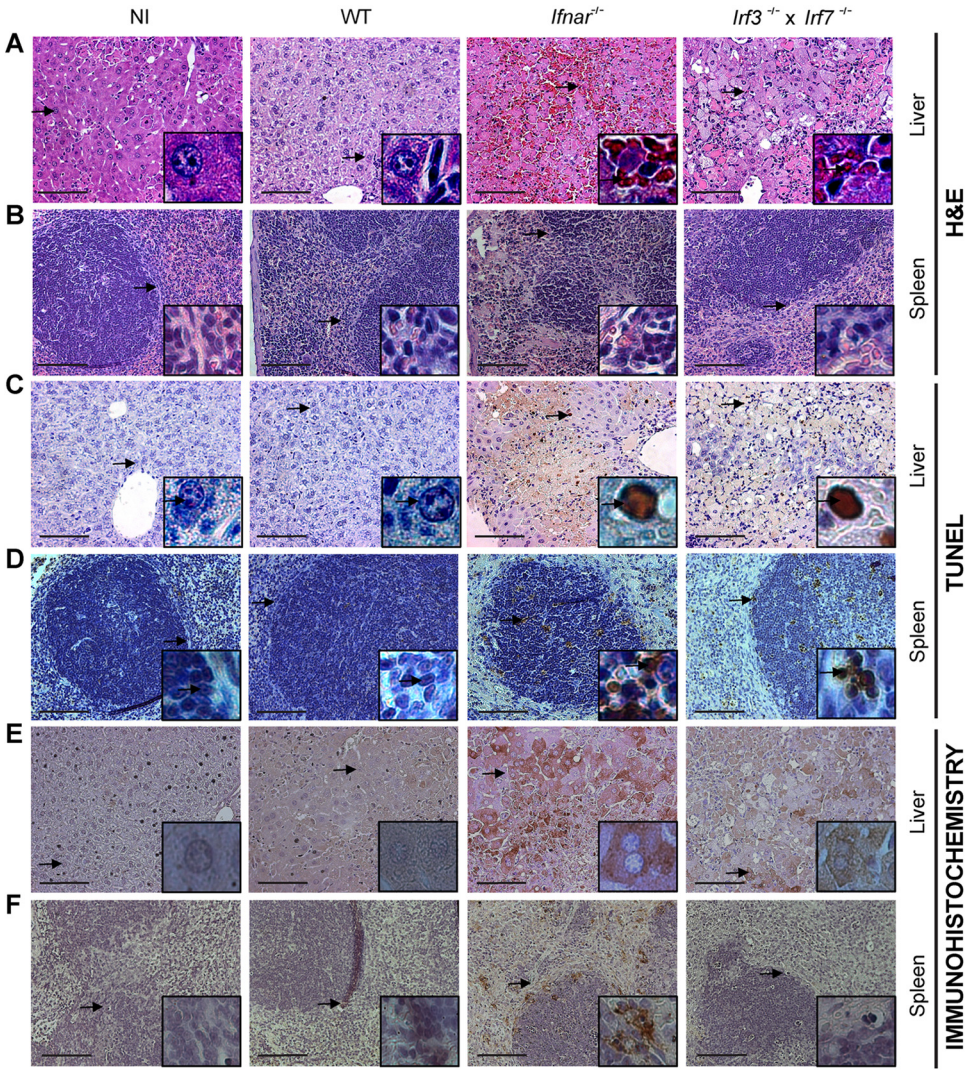

FIG 4 Tissue analysis of OROV-infected WT, *Ifnar*$^{-/-}$, and *Irf3*$^{-/-}$ × *Irf7*$^{-/-}$ DKO mice. (A and B) Histological (hematoxylin and eosin staining) analysis of the liver (A) and spleen (B) from uninfected WT mice and OROV-infected WT, *Ifnar*$^{-/-}$, or *Irf3*$^{-/-}$ × *Irf7*$^{-/-}$ DKO mice. Representative images (20× magnification) were taken 4 days after OROV infection from 3 mice of each group. (C and D) Representative images of TUNEL staining of liver (C) and spleen (D) of uninfected WT and infected WT, *Ifnar*$^{-/-}$, and *Irf3*$^{-/-}$ × *Irf7*$^{-/-}$ DKO mice were taken 4 days after OROV infection from 3 mice from each group. (E and F) Detection of OROV antigen in liver (E) and spleen (F) of uninfected WT and infected WT, *Ifnar*$^{-/-}$, and *Irf3*$^{-/-}$ × *Irf7*$^{-/-}$ DKO mice 4 days after virus infection. Representative images (taken at 20× magnification but decreased by 20% of their original size to fit) were obtained from three mice of each group. Inset images show a higher magnification image (taken at 40× magnification) and correspond to the region marked by the arrow. Scale bar, 100 μm.

while specific components of the IFN induction and signaling pathways restrict OROV in all cell types, their inhibitory effect is more dominant in myeloid cells, at least in culture.

OROV induces type I IFN production in mouse cells. Although several members of the *Orthobunyavirus* genera, including LACV, SBV, and BUNV, inhibit induction of type I IFN (33, 34, 55), we hypothesized that OROV might lack this activity in murine cells, which could explain its failure to cause disease in WT immunocompetent mice or replicate efficiently in some of the WT primary cells. To test this hypothesis, we infected WT, *Ifnar*$^{-/-}$, *Mavs*$^{-/-}$, and *Irf3*$^{-/-}$ × *Irf7*$^{-/-}$ DKO MEFs with OROV and measured *Ifna* and *Ifnb* mRNA levels by qRT-PCR after 1, 4, 12, 24, and 36 h. In parallel, we measured mRNA levels of *Ifit1*, a strongly induced ISG, and *Gapdh*; the latter gene serves as a control for possible virus-induced host transcriptional shutoff (Fig. 7A). We infected WT MEFs, as a positive control, with West Nile virus (WNV), an encephalitic flavivirus that potently induces type I IFN (52). In contrast to that seen with BUNV in either murine or human 293 cells (37), OROV infection did not inhibit type I IFN or ISG induction in WT MEFs, as induction of *Ifna*, *Ifnb*, and *Ifit1* mRNA was observed within 4 h of infection (Fig. 7B to D). The production of these mRNA, however, was delayed and blunted in *Mavs*$^{-/-}$ and *Irf3*$^{-/-}$ × *Irf7*$^{-/-}$ DKO MEFs (Fig. 7B to D), indicating that RLR signaling through IRF-3 and IRF-7 had a dominant effect on IFN and ISG induction. Consistent with this, we did not detect IFN-β protein by ELISA in the supernatants of *Mavs*$^{-/-}$ or *Irf3*$^{-/-}$ × *Irf7*$^{-/-}$ DKO MEFs, whereas high levels were observed in OROV-infected WT and *Ifnar*$^{-/-}$ cells (Fig. 7E). In *Mavs*$^{-/-}$ but not *Irf3*$^{-/-}$ × *Irf7*$^{-/-}$ DKO cells, *Ifit1* mRNA still accumulated, suggesting an RLR-independent pathway of induc-

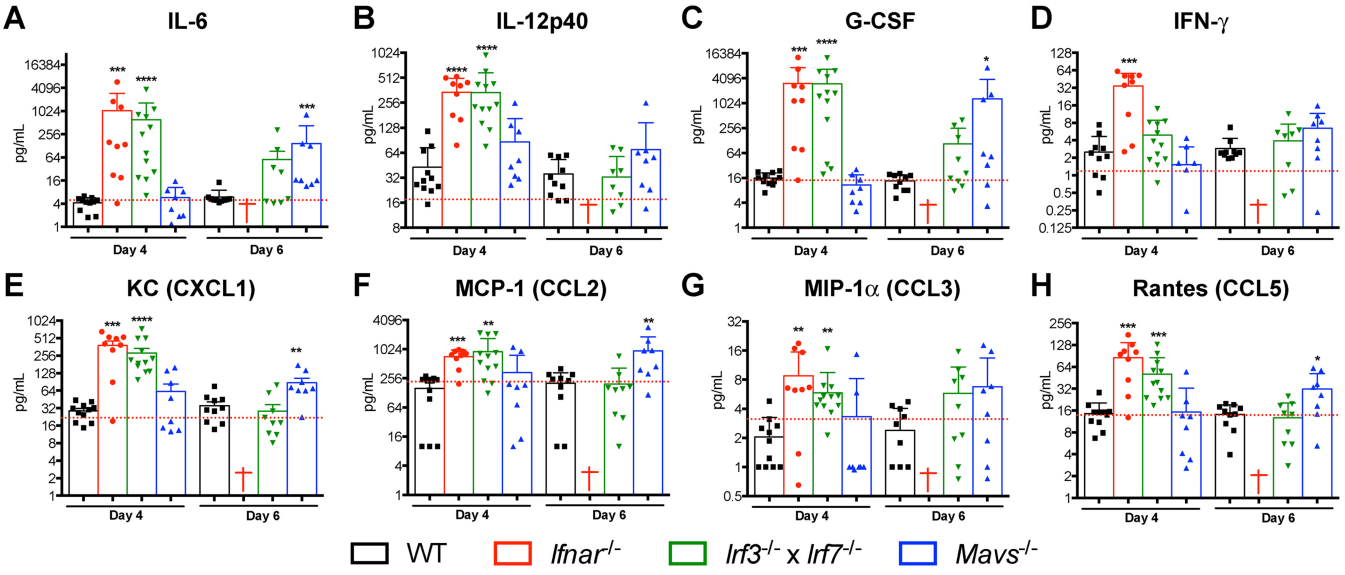

FIG 5 Serum cytokine and chemokine levels in OROV-infected mice. WT, *Ifnar*$^{-/-}$, *Irf3*$^{-/-}$ × *Irf7*$^{-/-}$, and *Mavs*$^{-/-}$ mice were infected with 10^6 FFU of OROV. Four or 6 days later, serum was collected and the concentrations of the indicated cytokines (A to D) or chemokines (E to H) were determined by Bio-Plex assay. Data points represent individual mice, and the bars indicate the mean values ± standard deviations (SD) for each group. A red cross indicates that all OROV-infected *Ifnar*$^{-/-}$ animals were dead at the indicated time point. Asterisks indicate statistical significance compared to serum from OROV-infected WT mice as judged by the Mann-Whitney test (*, $P < 0.05$; **, $P < 0.01$; ***, $P < 0.001$; ****, $P < 0.0001$). The red dotted lines represent the mean values from three mock-infected mice for each analyzed cytokine.

tion, possibly through TLRs (e.g., TLR3). *Ifit1* mRNA levels were abolished in OROV-infected *Ifnar*$^{-/-}$ MEFs (Fig. 7D) despite the increased level of infection, suggesting that the IFN-independent (e.g., IRF3-dependent [56]) pathway of ISG induction could not compensate for the loss of type I IFN signaling. These results indicate that OROV does not antagonize type I IFN production or signaling efficiently in mouse fibroblasts.

In comparison, the production of *IFNA*, *IFNB*, and *IFIT1* mRNAs after OROV infection was blunted in both 2fTGH and U3A (a 2fTGH-derived cell lacking STAT1) human fibrosarcoma cells relative to *GAPDH* expression or WNV infection (Fig. 7F to H; data not shown). Consistent with this attenuated IFN response, OROV replicated equally well in both cells lines (Fig. 7I). In particular, low levels of the ISG *IFIT1* were observed in OROV-infected cells, which suggests a virus-mediated defect in IFN-dependent or independent induction pathways. Thus, OROV appears to antagonize type I IFN production or signaling more efficiently in human cells than in mouse cells, which could explain why IFN induction and signaling are key restriction components in the murine model.

Type I IFN signaling in nonmyeloid cells likely contributes to defense against infection by OROV. As a deficiency of IFNAR signaling resulted in enhanced OROV infection of myeloid cells in culture, we evaluated its contribution to pathogenesis by infecting LysM Cre$^+$ *Ifnar*$^{f/f}$, CD11c Cre$^+$ *Ifnar*$^{f/f}$, and Cre$^-$ *Ifnar*$^{f/f}$ mice, which selectively delete IFNAR expression on Mϕ, monocytes, and granulocytes (LysM) or CD11c$^+$ DCs (57, 58). Unexpectedly, LysM Cre$^+$ *Ifnar*$^{f/f}$ and CD11c Cre$^+$ *Ifnar*$^{f/f}$ clinically were not more vulnerable to OROV infection; mortality rates and weight loss were similar to those for OROV-infected Cre$^-$ *Ifnar*$^{f/f}$ or WT mice (Fig. 8A and B). As observed in WT mice (see Fig. 2), infectious OROV was not detected in any tissue from LysM Cre$^+$ *Ifnar*$^{f/f}$, CD11c Cre$^+$ *Ifnar*$^{f/f}$, or Cre$^-$ *Ifnar*$^{f/f}$ mice on day 4 after infection by focus-forming assay (data not shown). However, using a more sensitive qRT-PCR assay that detects viral mRNAs and genomes, higher levels of OROV RNA were measured in the spleen of LysM Cre$^+$ *Ifnar*$^{f/f}$ ($P < 0.004$) and CD11c Cre$^+$ *Ifnar*$^{f/f}$ ($P < 0.05$) mice than Cre$^-$ *Ifnar*$^{f/f}$ or WT mice (Fig. 8C), suggesting that the deletion of IFNAR expression in myeloid cells facilitated OROV replication *in vivo*, but this was not sufficient to change the clinical outcome. Indeed, the levels of OROV RNA in the liver and serum were similar among all groups of animals (Fig. 8C and D). By inference, these results suggest that type I IFN signaling in nonmyeloid cells contributes to restricting OROV pathogenesis *in vivo*.

To assess whether myeloid cell types have a significant role in restricting infection by other orthobunyaviruses *in vivo*, we infected LysM Cre$^+$ *Ifnar*$^{f/f}$, CD11c Cre$^+$ *Ifnar*$^{f/f}$, Cre$^-$ *Ifnar*$^{f/f}$, *Ifnar*$^{-/-}$, and WT mice with 10^5 or 10^6 FFU of LACV. Similar to results reported previously (34, 36, 37), uniform and rapid lethality was observed after LACV infection of *Ifnar*$^{-/-}$ mice lacking type I IFN signaling in all cell types (Fig. 8E and F). Analogous to the results seen with OROV, CD11c Cre$^+$ *Ifnar*$^{f/f}$ mice did not show substantially enhanced lethality after LACV infection compared to Cre$^-$ *Ifnar*$^{f/f}$ and WT mice at either LACV dose (Fig. 8E and F). A significant weight loss in LACV-infected CD11c Cre$^+$ *Ifnar*$^{f/f}$ mice occurred late, on days 10 and 12, and only after infection with 10^6 FFU of LACV (Fig. 8G and H). Unexpectedly, LysM Cre$^+$ *Ifnar*$^{f/f}$ mice were more resistant to lethal LACV infection than WT or Cre$^-$ *Ifnar*$^{f/f}$ mice (Fig. 8F), suggesting that type I IFN signaling in Mϕ, monocytes, or granulocytes has a role in the pathogenesis induced by LACV. Independent of the differences in outcome, these results suggest that type I IFN signaling on nonmyeloid cells contributes to controlling infection of different orthobunyaviruses.

To corroborate the importance of type I IFN signaling in non-

TABLE 2 Serum cytokine and chemokine levels after OROV infection[a]

Cytokine	Genotype	Day 4 p.i.		Day 6 p.i.	
		pg/ml (±SD)	*P*	pg/ml (±SD)	*P*
IL-1α	WT	1.3 (±1.6)		2.6 (±2.3)	
	Ifnar$^{-/-}$	5.3 (±8.3)	0.93		
	Irf3$^{-/-}$ × *Irf7*$^{-/-}$	10.6 (±11.5)	0.08	0.6 (±1.4)	0.05
	Mavs$^{-/-}$	0 (±0)	0.03	5.4 (±7.8)	0.96
IL-1β	WT	189.4 (±44.2)		208.2 (±53.4)	
	Ifnar$^{-/-}$	266.0 (±179.8)	0.54		
	Irf3$^{-/-}$ × *Irf7*$^{-/-}$	205.7 (±135.5)	0.99	109.1 (±101.3)	0.04
	Mavs$^{-/-}$	123.5 (±95.1)	0.07	88.9 (±101.5)	0.02
IL-2	WT	25.0 (±14.6)		26.9 (±21.9)	
	Ifnar$^{-/-}$	18.9 (±11.3)	0.55		
	Irf3$^{-/-}$ × *Irf7*$^{-/-}$	20.9 (±14.1)	0.51	14.9 (±11.9)	0.50
	Mavs$^{-/-}$	16.6 (±12.8)	0.05	28.3 (±12.7)	0.22
IL-3	WT	12.8 (±11.9)		16.5 (±13.3)	
	Ifnar$^{-/-}$	5.13 (±7.19)	0.15		
	Irf3$^{-/-}$ × *Irf7*$^{-/-}$	8.6 (±9.9)	0.68	4.6 (±7.1)	0.09
	Mavs$^{-/-}$	3.6 (±3.3)	0.17	2.0 (±3.1)	0.008
IL-4	WT	6.9 (±8.4)		8.6 (±9.1)	
	Ifnar$^{-/-}$	2.5 (±3.9)	0.30		
	Irf3$^{-/-}$ × *Irf7*$^{-/-}$	3.0 (±5.7)	0.20	2.1 (±5.0)	0.32
	Mavs$^{-/-}$	0 (±0)	0.06	0 (±0)	0.03
IL-5	WT	14.3 (±7.5)		16.2 (±7.1)	
	Ifnar$^{-/-}$	10.2 (±3.1)	0.15		
	Irf3$^{-/-}$ × *Irf7*$^{-/-}$	6.2 (±4.2)	0.004	9.2 (±10.2)	0.17
	Mavs$^{-/-}$	8.8 (±5.8)	0.15	3.5 (±5.8)	0.002
IL-6	WT	4.2 (±1.5)		5.9 (±2.9)	
	Ifnar$^{-/-}$	1,048 (±1,921)	0.00008		
	Irf3$^{-/-}$ × *Irf7*$^{-/-}$	606 (±1,055)	<0.0001	56.8 (±107.4)	0.76
	Mavs$^{-/-}$	5.8 (±4.8)	0.64	146.1 (±279.1)	0.0002
IL-9	WT	108.6 (±115.4)		116.5 (±131.9)	
	Ifnar$^{-/-}$	337.9 (±410.3)	0.36		
	Irf3$^{-/-}$ × *Irf7*$^{-/-}$	159.7 (±282.9)	0.68	0 (±0)	0.03
	Mavs$^{-/-}$	96.3 (±167.6)	0.64	325.6 (±425.8)	0.45
IL-10	WT	22.8 (±16.3)		25.6 (±14.1)	
	Ifnar$^{-/-}$	23.8 (±14.6)	0.75		
	Irf3$^{-/-}$ × *Irf7*$^{-/-}$	31.6 (±35.1)	0.63	10.9 (±6.9)	0.01
	Mavs$^{-/-}$	17.4 (±17.0)	0.31	16.7 (±15.0)	0.18
IL-12 (p40)	WT	42.8 (±30.9)		35.4 (±17.6)	
	Ifnar$^{-/-}$	341.7 (±164.1)	<0.0001		
	Irf3$^{-/-}$ × *Irf7*$^{-/-}$	338.7 (±248.8)	<0.0001	32.6 (±25.1)	0.58
	Mavs$^{-/-}$	86.5 (±79.2)	0.09	69.7 (±77.6)	0.35
IL-12 (p70)	WT	18.6 (±12.2)		21.3 (±8.7)	
	Ifnar$^{-/-}$	74.5 (±93.6)	0.51		
	Irf3$^{-/-}$ × *Irf7*$^{-/-}$	33.8 (±31.2)	0.81	13.3 (±11.9)	0.11
	Mavs$^{-/-}$	14.6 (±11.6)	0.55	21.8 (±29.0)	0.17
IL-13	WT	31.6 (±26.3)		47.6 (±52.2)	
	Ifnar$^{-/-}$	30.3 (±31.9)	0.97		
	Irf3$^{-/-}$ × *Irf7*$^{-/-}$	47.2 (±61.9)	0.72	10.19 (±15.0)	0.04
	Mavs$^{-/-}$	14.0 (±25.4)	0.052	12.3 (±13.3)	0.03

(Continued on following page)

TABLE 2 (Continued)

Cytokine	Genotype	Day 4 p.i. pg/ml (±SD)	*P*	Day 6 p.i. pg/ml (±SD)	*P*
IL-17	WT	7.7 (±5.1)		8.7 (±6.6)	
	Ifnar$^{-/-}$	5.3 (±5.9)	0.15		
	Irf3$^{-/-}$ × *Irf7*$^{-/-}$	5.0 (±4.7)	0.12	5.1 (±4.3)	0.28
	Mavs$^{-/-}$	2.5 (±2.1)	0.02	2.4 (±1.6)	0.07
Eotaxin	WT	422.5 (±287.0)		478.5 (±230.7)	
	Ifnar$^{-/-}$	451.5 (±462.0)	0.84		
	Irf3$^{-/-}$ × *Irf7*$^{-/-}$	344.2 (±292.9)	0.42	178.5 (±170.8)	0.005
	Mavs$^{-/-}$	145.1 (±189.2)	0.03	180.2 (±206.0)	0.01
G-CSF	WT	15.8 (±5.2)		13.6 (±5.5)	
	Ifnar$^{-/-}$	3,064 (±4,307)	0.0004		
	Irf3$^{-/-}$ × *Irf7*$^{-/-}$	3,000 (±3,767)	<0.0001	106.7 (±146.5)	0.09
	Mavs$^{-/-}$	10.8 (±8.2)	0.15	1,307 (±2,543)	0.03
GM-CSF	WT	70.8 (±26.6)		74.8 (±29.3)	
	Ifnar$^{-/-}$	86.5 (±32.8)	0.12		
	Irf3$^{-/-}$ × *Irf7*$^{-/-}$	63.5 (±23.9)	0.43	57.6 (±39.7)	0.23
	Mavs$^{-/-}$	43.9 (±19.1)	0.06	22.0 (±28.3)	0.03
IFN-γ	WT	2.5 (±2.1)		2.8 (±1.4)	
	Ifnar$^{-/-}$	34.2 (±22.8)	0.0004		
	Irf3$^{-/-}$ × *Irf7*$^{-/-}$	4.9 (±3.9)	0.11	3.9 (±3.7)	0.94
	Mavs$^{-/-}$	1.5 (±1.5)	0.29	6.4 (±5.1)	0.10
KC	WT	28.7 (±9.5)		35.3 (±18.7)	
	Ifnar$^{-/-}$	384.2 (212.1)	0.0008		
	Irf3$^{-/-}$ × *Irf7*$^{-/-}$	285.5 (196.0)	<0.0001	28.5 (±24.6)	0.23
	Mavs$^{-/-}$	61.6 (±59.9)	0.79	87.6 (±48.8)	0.008
MCP-1	WT	156.1 (±113.0)		202.0 (±132.8)	
	Ifnar$^{-/-}$	716.6 (±267.5)	0.0003		
	Irf3$^{-/-}$ × *Irf7*$^{-/-}$	902.8 (±786.5)	0.0026	195.2 (±221.3)	0.39
	Mavs$^{-/-}$	335.5 (±435.0)	0.98	946.6 (±903.8)	0.0043
MIP-1α	WT	1.6 (±1.5)		2.1 (±1.9)	
	Ifnar$^{-/-}$	8.8 (±6.6)	0.004		
	Irf3$^{-/-}$ × *Irf7*$^{-/-}$	5.8 (±3.6)	0.0001	5.6 (±5.1)	0.13
	Mavs$^{-/-}$	2.7 (±5.2)	0.52	6.6 (±6.8)	0.12
MIP-1β	WT	36.6 (±22.8)		45.2 (±20.4)	
	Ifnar$^{-/-}$	35.0 (±24.0)	0.91		
	Irf3$^{-/-}$ × *Irf7*$^{-/-}$	23.7 (±12.3)	0.21	38.8 (±36.6)	0.71
	Mavs$^{-/-}$	31.5 (±16.2)	0.69	18.5 (±16.9)	0.03
RANTES	WT	14.5 (±5.8)		14.1 (±5.1)	
	Ifnar$^{-/-}$	85.6 (±52.3)	0.0008		
	Irf3$^{-/-}$ × *Irf7*$^{-/-}$	50.9 (±34.5)	0.0001	12.6 (±7.6)	0.64
	Mavs$^{-/-}$	15.3 (±17.1)	0.30	31.6 (±19.8)	0.04
TNF-α	WT	276.4 (±193.8)		334.2 (±182.7)	
	Ifnar$^{-/-}$	198.4 (±117.9)	0.36		
	Irf3$^{-/-}$ × *Irf7*$^{-/-}$	179.1 (±113.4)	0.20	145.2 (±101.3)	0.05
	Mavs$^{-/-}$	155.0 (±157.2)	0.17	137.3 (±114.5)	0.04

[a] The indicated strains of mice were infected with OROV. Serum was collected on days 4 and 6 postinfection (p.i.), and cytokines and chemokines were measured by Bio-Plex array. Data represent the means (±SD) in pg/ml from 8 to 12 mice per group. Statistical significance was determined using the Mann-Whitney test, and *P* values were obtained after comparison to infected WT mice.

myeloid cells in OROV pathogenesis, reciprocal bone marrow chimera and infection studies were performed. We adoptively transferred WT or *Ifnar*$^{-/-}$ bone marrow cells into sublethally irradiated 4-week-old *Ifnar*$^{-/-}$ or WT recipient mice (Fig. 9A). Eight weeks later, the reconstitution of donor immune cell populations in blood was confirmed in recipient mice by flow cytometry (Fig. 9B). All recipient animals were infected with OROV and 4 days later were analyzed. WT recipient animals receiving donor

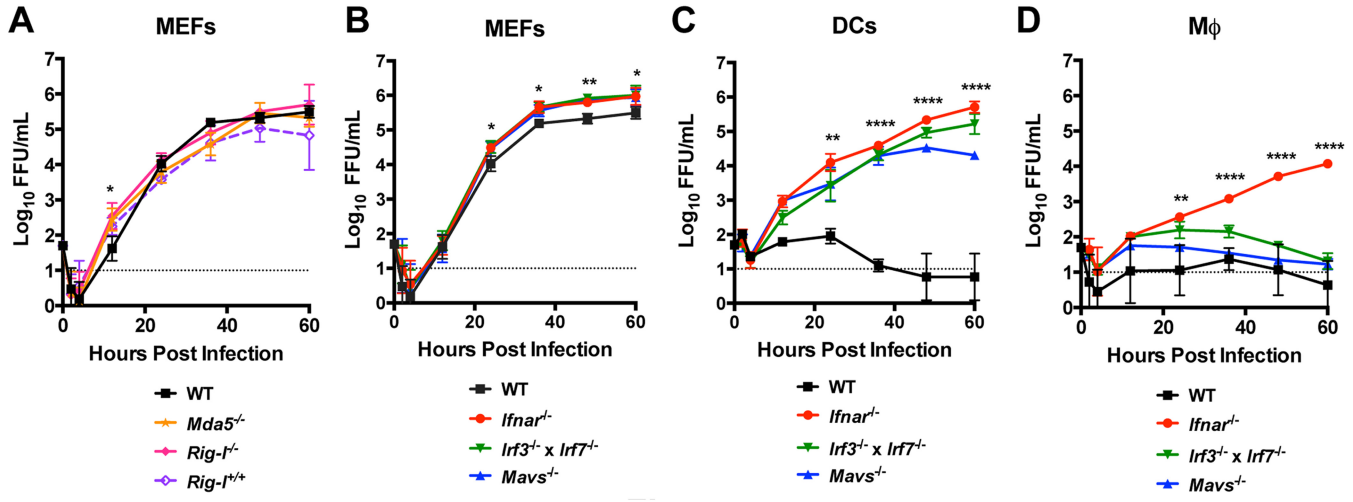

FIG 6 OROV replication in primary MEFs, DCs, and Mϕ. (A and B) Kinetics of OROV replication in WT, *Ifnar*$^{-/-}$, *Mavs*$^{-/-}$, and *Irf3*$^{-/-}$ × *Irf7*$^{-/-}$ MEFs (A) or *Rig-I*$^{-/-}$, *Rig-I*$^{+/+}$, and MDA5$^{-/-}$ MEFs (B) after infection at an MOI of 0.001. Supernatants were harvested at the indicated times for titration by focus-forming assay. (C and D) Kinetics of OROV replication in DCs (C) and Mϕ (D) derived from WT, *Ifnar*$^{-/-}$, *Mavs*$^{-/-}$, and *Irf3*$^{-/-}$ × *Irf7*$^{-/-}$ mice after infection at an MOI of 0.001. The data represent the means ± SD from three independent experiments performed in triplicate. All KO cell groups were compared to WT by two-way ANOVA, and asterisks indicate statistical significance (*, $P < 0.05$; **, $P < 0.01$; ***, $P < 0.001$; ****, $P < 0.0001$). The dotted line represents the limit of detection of the assay.

bone marrow cells from either WT or *Ifnar*$^{-/-}$ mice showed no macroscopic evidence of liver injury. Consistent with this observation, these recipient animals had only mildly elevated serum transaminases (AST and ALT), normal glucose levels in serum, and little evidence of OROV infection in the liver or spleen (Fig. 9C and D). In contrast, OROV-infected *Ifnar*$^{-/-}$ mice that had received WT donor bone marrow sustained liver injury that was equivalent to that in unmanipulated *Ifnar*$^{-/-}$ mice, with markedly elevated AST and ALT levels, hypoglycemia, and high levels of OROV infection. These studies support a protective role of IFNAR signaling in radio-resistant nonmyeloid cells during OROV infection.

DISCUSSION

In this study, we evaluated the mechanisms of innate immune control of OROV, an emerging insect-transmitted orthobunyavirus of global concern. Our experiments suggest that pathogen recognition by RLR family members, activation of MAVS, IRF-3, and IRF-7, and production of type I IFN help to orchestrate control of OROV replication in mice. As evidence of this, although 6-week-old WT C57BL/6 mice were resistant to OROV infection and did not sustain appreciable infectious titers in their organs, a high proportion of *Ifnar*$^{-/-}$, *Mavs*$^{-/-}$, and *Irf3*$^{-/-}$ × *Irf7*$^{-/-}$ DKO mice succumbed to lethal infection by a subcutaneous injection route and developed high levels of virus in the liver, spleen, and blood.

Our results demonstrate that an IFN-induced antiviral state against OROV was triggered downstream of MAVS activation and IRF-3- and IRF-7-mediated transcription, although some *Mavs*$^{-/-}$ and *Irf3*$^{-/-}$ × *Irf7*$^{-/-}$ DKO mice survived and cleared the virus infection. It is likely that both IFN-α and IFN-β contribute to protection against OROV infection, since only a small proportion of *Ifnb*$^{-/-}$ mice succumbed to viral infection, whereas all *Ifnar*$^{-/-}$ mice died rapidly. Analogously, *Ifnb*$^{-/-}$ mice exhibited an intermediate survival phenotype when infected with the related LACV (35) or unrelated WNV (59). A recent study on LACV showed that activation of MAVS led to upregulation of the adaptor protein SARM1 and increased neuronal death via oxidative stress and mitochondrial damage (40). In that study, *Mavs*$^{-/-}$ mice showed decreased lethality compared to that of WT mice, although viral yields in the brain were unchanged. Our results differ in that *Mavs*$^{-/-}$ mice were more vulnerable to OROV infection and sustained higher titers in the liver than WT mice. Although direct comparative experiments are warranted, the disparity in the MAVS-dependent phenotype between the two studies could reflect experimental variables, including the age of the mice (3 versus 6 weeks old), the route of inoculation (intraperitoneal versus subcutaneous), and the input dose (10^3 versus 10^6 FFU) or inherent differences in pathogenicity and tropism of OROV and LACV.

IRF-3 and IRF-7 are transcription factors that regulate expression of type I IFN and ISGs (56, 60). Although IRF-3 is expressed constitutively in many cell types, apart from a subset of cells, including plasmacytoid DCs, IRF-7 expression is induced by IRF-3 or IFNAR signaling (61). The nonredundant roles of IRF-3 and IRF-7 have been documented in pathogenesis studies with other viruses (47, 62). Consistent with this, we observed no lethality of *Irf3*$^{-/-}$ or *Irf7*$^{-/-}$ single-KO mice after OROV infection, whereas ~50% of *Irf3*$^{-/-}$ × *Irf7*$^{-/-}$ DKO mice succumbed to infection and exhibited greater viral burden. Nonetheless, the *Irf3*$^{-/-}$ × *Irf7*$^{-/-}$ DKO mice did not phenocopy *Ifnar*$^{-/-}$ mice. OROV also replicated to higher levels in *Ifnar*$^{-/-}$ DCs and Mϕ than in *Irf3*$^{-/-}$ × *Irf7*$^{-/-}$ cells. These data suggest that other transcription factors likely contribute to type I IFN induction after OROV infection. IRF-1 and IRF-5 are candidate factors, as they have been shown to regulate type I IFN responses against viruses under some circumstances (52, 63–66).

In our immunocompromised mouse models of OROV infection, we observed hepatic injury and necrosis that likely caused lethal disease, which was not observed in WT mice. This disease

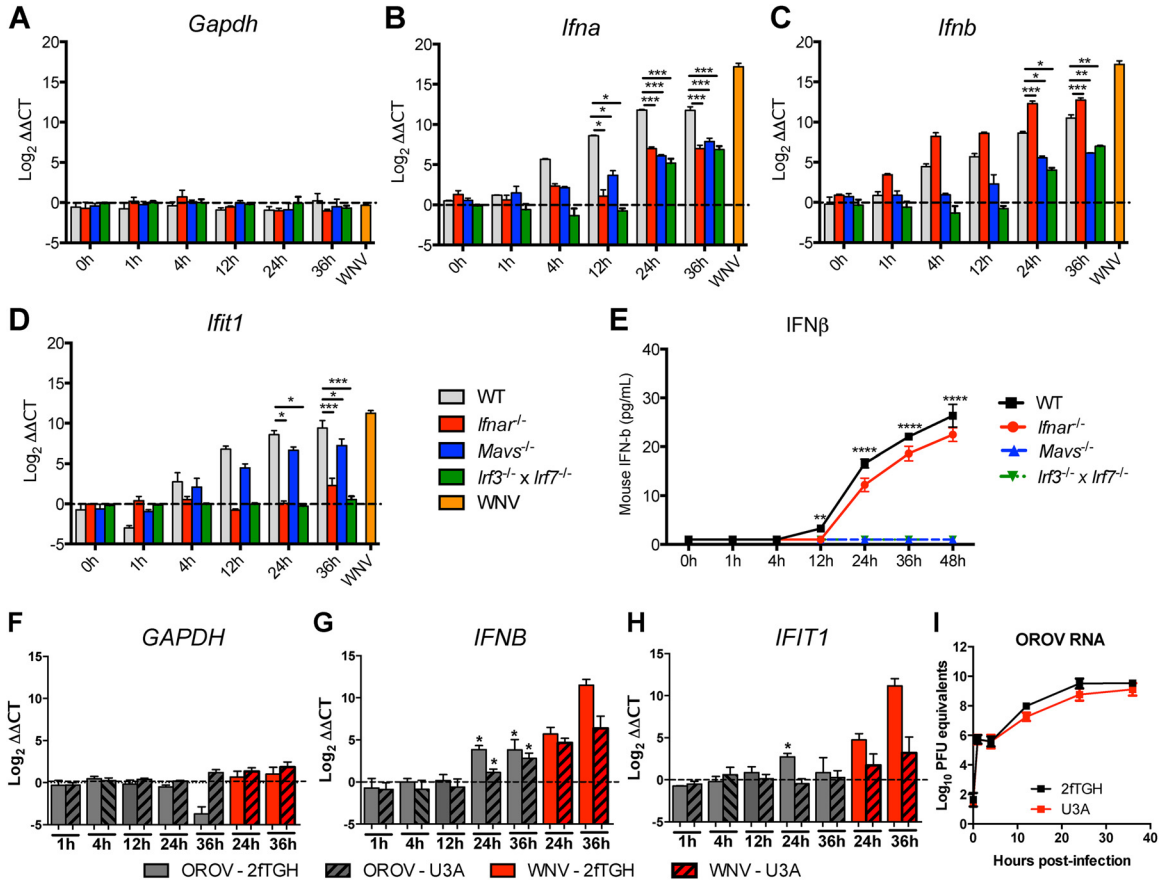

FIG 7 OROV efficiently induces type I IFN production and ISGs in murine but not in human cells. (A to D) MEFs from WT, *Ifnar*$^{-/-}$, *Mavs*$^{-/-}$, and *Irf3*$^{-/-}$ × *Irf7*$^{-/-}$ mice were infected with OROV at an MOI of 0.1 or mock infected. At 1, 4, 12, or 36 h after infection, the relative expression levels of *Gapdh* (A), *Ifna* (B), *Ifnb* (C), and *Ifit1* (D) mRNA were determined by qRT-PCR. Gene expression was normalized to 18S rRNA and is displayed as the fold increase compared to the mock-infected cells on a $\log_2$ scale. Data represent the averages from three independent experiments performed in triplicate and are expressed as the means ± SD. (E) MEFs from WT, *Ifnar*$^{-/-}$, *Mavs*$^{-/-}$, and *Irf3*$^{-/-}$ × *Irf7*$^{-/-}$ mice were infected with OROV at an MOI of 0.1. At 1, 4, 12, 36, and 48 h after infection, the accumulation of IFN-β protein in the supernatant was determined by ELISA. The results are expressed in pg/ml after plotting the optical densities using a 4-parameter fit for the standard curve run in the same plate. The data represent the means ± SD from two independent experiments performed in triplicate. (F to H) 2fTGH and U3A human cells were infected with OROV at an MOI of 0.1 or mock infected. At 1, 4, 12, or 36 h after infection, the relative expression levels of *GAPDH* (F), *IFNB* (G), and *IFIT1* (H) mRNA were determined by qRT-PCR. Gene expression was normalized to 18S rRNA and is displayed as the fold increase compared to the mock-infected cells on a $\log_2$ scale. (I) Kinetics of OROV replication in 2fTGH and U3A human cells after infection at an MOI of 0.1. The cells were lysed and harvested at the indicated times for RNA extraction and qRT-PCR. The data represent the means ± SD from three independent experiments performed in triplicate. In this figure, asterisks indicate statistical significance (*, $P < 0.05$; **, $P < 0.01$; ***, $P < 0.001$; ****, $P < 0.0001$), and the dotted line represents the limit of detection of the assay.

manifested histologically as TUNEL$^+$ hepatocytes and by the high levels of liver transaminases and low level of glucose in serum. In humans, this extensive degree of liver injury is not typical, although elevated liver transaminases in serum of patients with OROV fever have been reported (12). Although some aspects of OROV disease in the KO mice do not clearly parallel human infection, the development of subcutaneous infection mouse models of OROV likely will be useful in monitoring effects on viral replication in the context of future preclinical testing of therapeutics, akin to studies with the unrelated dengue virus (DENV), which also replicates poorly in WT mice (reviewed in reference 67).

Because our histopathological and blood chemistry studies showed massive liver damage after OROV infection of immunocompromised mice, we hypothesized this might be due to sepsis and cytokine storm, as we observed previously with the flavivirus WNV (51). Although we detected an elevation in the levels of several cytokines and chemokines (e.g., IL-6, IL-12p40, G-CSF, KC, MCP-1, MIP-1α, and RANTES) in *Ifnar*$^{-/-}$, *Mavs*$^{-/-}$, and *Irf3*$^{-/-}$ × *Irf7*$^{-/-}$ DKO mice on days 4 and 6 after OROV infection, the vasoactive cytokines TNF-α and IL-1β were within the normal range. Also inconsistent with a cytokine storm scenario and sepsis physiology, we failed to observe significant renal damage, as judged by normal blood urea nitrogen and serum creatinine values. Together with our viral burden and immunohistochemical analyses, it seems more likely that the liver damage in OROV-infected *Ifnar*$^{-/-}$, *Mavs*$^{-/-}$, and *Irf3*$^{-/-}$ × *Irf7*$^{-/-}$ DKO mice was due to the direct cytopathic effects of the virus in hepatocytes. Alternatively, although further study is necessary, immune cell targeting of virally infected cells by natural killer or cytotoxic T cells could contribute to acute liver damage. The etiology of liver damage and its role in orthobunyavirus pathogenesis remain to be completely understood, although OROV and Melao virus (MELV) infection directly infect the liver in hamsters (21,

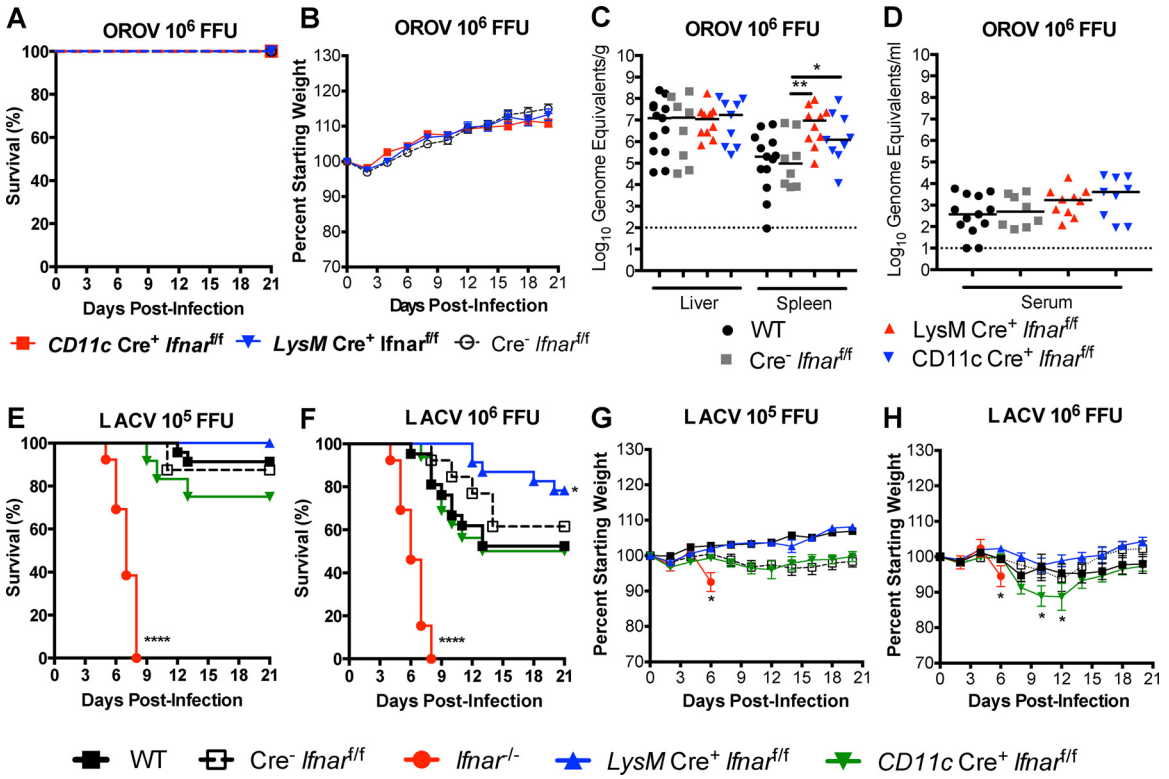

FIG 8 LysM Cre$^+$ *Ifnar*$^{f/f}$ and CD11c Cre$^+$ *Ifnar*$^{f/f}$ are not more vulnerable to OROV and LACV infection. (A) Survival analysis of 5- to 6-week-old mice after inoculation with 10^6 FFU of OROV by footpad injection: CD11c Cre$^+$ *Ifnar*$^{f/f}$ ($n = 30$), LysM Cre$^+$ *Ifnar*$^{f/f}$ ($n = 25$), and Cre$^-$ *Ifnar*$^{f/f}$ ($n = 31$) mice were used to construct survival curves. Data are pooled from at least three independent experiments. (B) Weight loss in CD11c Cre$^+$ *Ifnar*$^{f/f}$ ($n = 30$), LysM Cre$^+$ *Ifnar*$^{f/f}$ ($n = 25$), and Cre$^-$ *Ifnar*$^{f/f}$ ($n = 31$) mice. The weight loss curves were compared at a given time point using 2-way ANOVA. (C and D) Quantification of OROV RNA by qRT-PCR in the liver (C), spleen (C), and serum (D) from WT, CD11c Cre$^+$ *Ifnar*$^{f/f}$, LysM Cre$^+$ *Ifnar*$^{f/f}$, and Cre$^-$ *Ifnar*$^{f/f}$ mice at 4 days after infection. A scatter plot of the data is shown, with each point representing a single animal. The bars indicate median values and were obtained from 10 mice per group. The dotted line represents the limit of detection of the assay. Groups were compared to the WT by the Mann-Whitney test; asterisks indicate statistically significant differences (*, $P < 0.05$; **, $P < 0.01$). Note, OROV RNA was detected in the serum, spleen, and liver of WT mice by qRT-PCR, as this assay was more sensitive than infectious virus titration (Fig. 2) or IHC (Fig. 4). (E and F) Survival analysis of 8-week-old mice after inoculation with 10^5 FFU ($n = 23$ for WT, $n = 5$ for *Ifnar*$^{-/-}$, $n = 25$ for LysM Cre$^+$ *Ifnar*$^{f/f}$, $n = 12$ for CD11c Cre$^+$ *Ifnar*$^{f/f}$, and $n = 8$ for Cre$^-$ *Ifnar*$^{f/f}$) (E) or 10^6 FFU ($n = 21$ for WT, $n = 5$ for *Ifnar*$^{-/-}$, $n = 23$ for LysM Cre$^+$ *Ifnar*$^{f/f}$, $n = 16$ for CD11c Cre$^+$ *Ifnar*$^{f/f}$, and $n = 13$ for Cre$^-$ *Ifnar*$^{f/f}$) (F) of LACV by footpad injection. (G and H) Weight loss analysis of 8-week-old mice after inoculation with 10^5 FFU (G) or 10^6 FFU (H) of LACV by footpad injection in the same mice. Data are pooled from at least three independent experiments. Survival curves were analyzed by the log rank test, and weight loss values were compared by 2-way ANOVA. Asterisks indicate differences that were statistically significant compared to WT animals with the same viral dose (*, $P < 0.05$).

68). Additional pathological mechanisms may contribute, as infection of mice with Caraparu virus (CARV), a member of group C of the *Bunyaviridae* family, induces acute oxidative stress-dependent hepatitis, with increased serum levels of AST and ALT (69).

Myeloid cell-dependent IFNAR signaling is essential for restricting pathogenesis of some (e.g., WNV, DENV, and mouse hepatitis viruses) (51, 70, 71) but not all (e.g., chikungunya virus) viruses (72). Somewhat unexpectedly, CD11c Cre$^+$ *Ifnar*$^{f/f}$ and LysM Cre$^+$ *Ifnar*$^{f/f}$ did not succumb to infection with 10^6 FFU of OROV or 10^5 FFU of LACV, suggesting that IFNAR signaling by nonmyeloid cell subtypes has a dominant role in restricting infection by these orthobunyaviruses. Bone marrow chimera studies revealed that IFNAR signaling in radio-resistant cells helps to restrict OROV infection and injury in the liver. It remains possible that IFNAR signaling in selected radio-resistant myeloid cell subsets (e.g., resident tissue macrophages) *in vivo* contributes to control of OROV infection. Moreover, IFN signaling in myeloid cells likely has some role in restricting orthobunyaviruses, as bone marrow-derived Mϕ and DCs from WT mice were relatively resistant to OROV infection, whereas cells from *Ifnar*$^{-/-}$ mice were susceptible. Consistent with this data, increased levels of OROV RNA were detected in the spleen of CD11c Cre$^+$ *Ifnar*$^{f/f}$ and LysM Cre$^+$ *Ifnar*$^{f/f}$ mice, and infection with LACV was associated with greater weight loss in CD11c Cre$^+$ *Ifnar*$^{f/f}$ mice. Indeed, a recent study demonstrated that myeloid dendritic cells are critical for the type I IFN response and protection to LACV in adult mice (73). Differences on routes of infection (subcutaneous versus intraperitoneal) and age of animals (8 versus 6 weeks old) may explain the disparity in mortality rates between the two studies in CD11c Cre$^+$ *Ifnar*$^{f/f}$ mice after LACV infection.

OROV is a zoonotic virus that circulates in vertebrate animals in South America, including sloths and monkeys. The ability of OROV to infect and replicate in wild rodents remains uncertain, but the seroprevalence rate is low (12). Productive infection by OROV in a mammalian host likely depends on several factors, including its ability to evade the innate immune response. Members of the *Bunyaviridae* family possess several mechanisms to

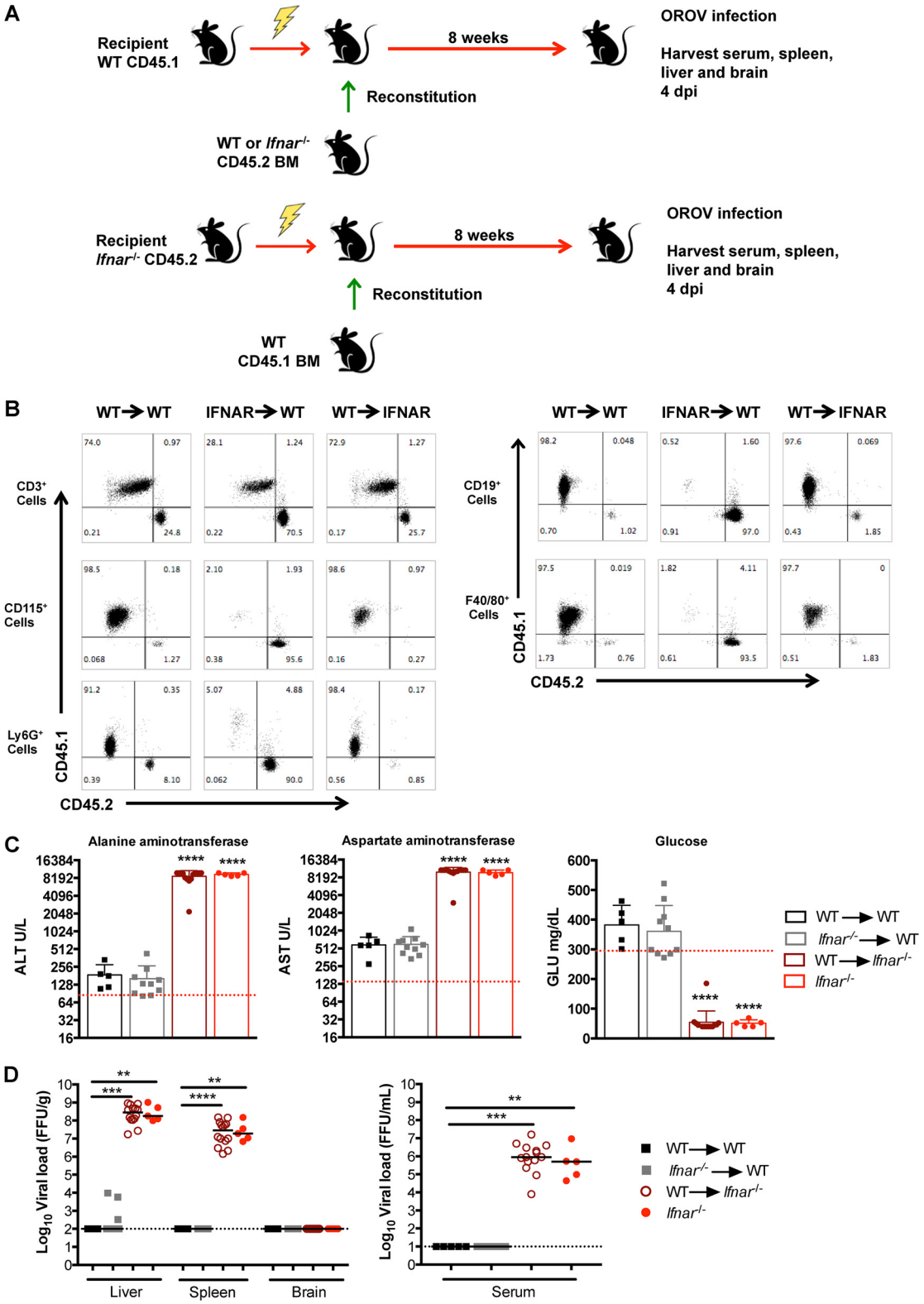

FIG 9 A deficiency of IFNAR expression on radio-resistant cells determines OROV pathogenesis. (A) Bone marrow cells from C57BL/6 WT or *Ifnar*$^{-/-}$ mice were transferred adoptively (10^7 cells per recipient animal) to 800-cGy-irradiated 4-week-old WT or *Ifnar*$^{-/-}$ mice (WT→WT, WT→*Ifnar*$^{-/-}$, *Ifnar*$^{-/-}$→WT). After validation of donor immune cell reconstitution (B), recipient animals were infected with 10^6 FFU of OROV. Four days later, serum, spleen, and liver were harvested for blood chemistry and viral titer analyses. Results were compared to data obtained in parallel experiments with OROV-infected unmanipulated *Ifnar*$^{-/-}$ mice. (C) Alanine aminotransferase (ALT), aspartate aminotransferase (AST), and glucose (GLU) levels were measured from serum of recipient WT and *Ifnar*$^{-/-}$ mice 4 days after OROV infection. Data points represent individual mice. Data are pooled from two independent experiments, and the asterisks indicate statistical significance as judged by the Mann-Whitney test (*, $P < 0.05$; **, $P < 0.01$; ***, $P < 0.001$; ****, $P < 0.0001$). (D) Quantification of OROV in the liver, spleen, brain, and serum from recipient WT and *Ifnar*$^{-/-}$ mice at 4 days after infection. A scatter plot of the data is shown, with each point representing a single animal. The bars indicate median values and were obtained from 5 to 14 mice per group. The dotted line represents the limit of detection of the assay. Groups were compared by the Mann-Whitney test; asterisks indicate statistically significant differences (**, $P < 0.01$; ***, $P < 0.001$).

antagonize the type I IFN and innate immune response pathways, primarily through the actions of N-terminal domains in the L protein or via their NSs protein. The L gene of CCHFV encodes an ovarian tumor (OUT) domain-containing viral protease that hydrolyzes ubiquitin and ISG15 from cellular target proteins, which leads to inhibition of NF-κB-dependent signaling and loss of antiviral effects of ISG15 (74). The NSs genes of orthobunyaviruses reportedly induce mammalian cell protein shutoff (33, 75), suppression of RNA interference (55), and inhibition of *IFNB* transcription and ISG production (33–35). Although NSs proteins are not essential for orthobunyavirus growth in tissue culture (reviewed in reference 76), they contribute to pathogenesis, as their deletion attenuates infection in mice, as seen for Akabane virus, BUNV, and LACV (33, 35, 37, 77). The recent development of an artificial minigenome system for OROV (78) will help to address which genes (L, NSs, or other genes) antagonize the type I IFN pathway to promote infection.

Our data suggest that OROV did not inhibit type I IFN production efficiently in mouse cells and, accordingly, virus infection was greater in cells deficient in IFN induction or signaling. Correspondingly, in WT mice, OROV infection was abortive, whereas high levels of replication and disease were sustained in *Ifnar*$^{-/-}$ or *Irf3*$^{-/-}$ × *Irf7*$^{-/-}$ animals. In contrast, at least in the two human cell lines that we tested, the induction of type I IFN or ISGs was diminished. One possible explanation for our findings, which requires confirmation, is a species-specific immune antagonism activity of OROV NSs (or L), which blocks human but not mouse IFN responses. This concept might explain the species barrier of OROV in immunocompetent rodents analogous to what has been described for other viruses, including DENV, where the viral NS2B3 and NS5 proteins promote degradation of human but not mouse STING and STAT2 (79–82). Alternatively, the attenuated phenotype in mice was due to the particular OROV strain we used. Future studies using OROV field isolates will be needed to address this issue more definitively.

In summary, our study establishes that the induction of type I IFN through MAVS, IRF-3, and IRF-7 is essential to control OROV infection in mice, and this likely occurs dominantly in nonmyeloid cells. The disease, associated with OROV infection of immunocompromised mice, caused marked hepatic injury. Given the extent of OROV infection in the liver of *Ifnar*$^{-/-}$ mice, hepatocytes may require IFN signaling to avoid targeting by OROV. The animal models described here may be useful for understanding the basic biology of OROV, an emerging infectious disease with epidemic potential, as well as testing new candidate therapeutics.

ACKNOWLEDGMENTS

The National Institutes of Health (R01 AI104972 to M.S.D and P30 DK52574 to Digestive Diseases Research Core Center Morphology Core), Conselho Nacional de Desenvolvimento Científico e Tecnológico (CNPq)–Science Without Borders (246513/2012-8 to J.L.P.-M), and a University Research Committee grant supported this work.

We gratefully acknowledge the technical assistance of Jennifer Govero, Michelle Noll, and Soila Sukupolvi-Petty.

REFERENCES

1. **Fauquet CM, Mayo MA, Maniloff J, Desselberger U, Ball LA.** 2005. Bunyaviridae, p 695–699. *In* Fauquet CM, Mayo MA, Maniloff J, Desselberger U, Ball LA (ed), Virus taxonomy classification and nomenclature of viruses. Eighth report of the International Committee on Taxonomy of Viruses. Virology division. International Union of Microbiological Societies. Elsevier, San Diego, CA.
2. **Santos RI, Rodrigues AH, Silva ML, Mortara RA, Rossi MA, Jamur MC, Oliver C, Arruda E.** 2008. Oropouche virus entry into HeLa cells involves clathrin and requires endosomal acidification. Virus Res **138:**139–143. http://dx.doi.org/10.1016/j.virusres.2008.08.016.
3. **Plassmeyer ML, Soldan SS, Stachelek KM, Martin-Garcia J, Gonzalez-Scarano F.** 2005. California serogroup Gc (G1) glycoprotein is the principal determinant of pH-dependent cell fusion and entry. Virology **338:** 121–132. http://dx.doi.org/10.1016/j.virol.2005.04.026.
4. **Patterson JL, Holloway B, Kolakofsky D.** 1984. La Crosse virions contain a primer-stimulated RNA polymerase and a methylated cap-dependent endonuclease. J Virol **52:**215–222.
5. **Mir MA, Panganiban AT.** 2006. The bunyavirus nucleocapsid protein is an RNA chaperone: possible roles in viral RNA panhandle formation and genome replication. RNA **12:**272–282. http://dx.doi.org/10.1261/rna.2101906.
6. **Jin H, Elliott RM.** 1993. Characterization of Bunyamwera virus S RNA that is transcribed and replicated by the L protein expressed from recombinant vaccinia virus. J Virol **67:**1396–1404.
7. **Schmaljohn CS, Nichol ST.** 2007. Bunyaviridae, p 1741–1778. *In* Knipe DM, Howley PM, Griffin DE (ed), Fields virology, vol 2. Lippincott Williams & Wilkins, Philadelphia, PA.
8. **Novoa RR, Calderita G, Cabezas P, Elliott RM, Risco C.** 2005. Key Golgi factors for structural and functional maturation of bunyamwera virus. J Virol **79:**10852–10863. http://dx.doi.org/10.1128/JVI.79.17.10852-10863.2005.
9. **Forshey BM, Guevara C, Laguna-Torres VA, Cespedes M, Vargas J, Gianella A, Vallejo E, Madrid C, Aguayo N, Gotuzzo E, Suarez V, Morales AM, Beingolea L, Reyes N, Perez J, Negrete M, Rocha C, Morrison AC, Russell KL, Blair PJ, Olson JG, Kochel TJ, NMRCD Febrile Surveillance Working Group.** 2010. Arboviral etiologies of acute febrile illnesses in Western South America, 2000-2007. PLoS Negl Trop Dis **4:**e787. http://dx.doi.org/10.1371/journal.pntd.0000787.
10. **Vasconcelos HB, Nunes MR, Casseb LM, Carvalho VL, Pinto da Silva EV, Silva M, Casseb SM, Vasconcelos PF.** 2011. Molecular epidemiology of Oropouche virus, Brazil. Emerg Infect Dis **17:**800–806. http://dx.doi.org/10.3201/eid1705.101333.
11. **Watts DM, Lavera V, Callahan J, Rossi C, Oberste MS, Roehrig JT, Cropp CB, Karabatsos N, Smith JF, Gubler DJ, Wooster MT, Nelson WM, Hayes CG.** 1997. Venezuelan equine encephalitis and Oropouche virus infections among Peruvian army troops in the Amazon region of Peru. Am J Trop Med Hyg **56:**661–667.
12. **Pinheiro FP, Travassos da Rosa AP, Travassos da Rosa JF, Ishak R, Freitas RB, Gomes ML, LeDuc JW, Oliva OF.** 1981. Oropouche virus. I. A review of clinical, epidemiological, and ecological findings. Am J Trop Med Hyg **30:**149–160.
13. **Aguilar PV, Barrett AD, Saeed MF, Watts DM, Russell K, Guevara C, Ampuero JS, Suarez L, Cespedes M, Montgomery JM, Halsey ES, Kochel TJ.** 2011. Iquitos virus: a novel reassortant Orthobunyavirus associated with human illness in Peru. PLoS Negl Trop Dis **5:**e1315. http://dx.doi.org/10.1371/journal.pntd.0001315.
14. **De Figueiredo RM, Thatcher BD, de Lima ML, Almeida TC, Alecrim WD, Guerra MV.** 2004. Exanthematous diseases and the first epidemic of dengue to occur in Manaus, Amazonas State, Brazil, during 1998-1999. Rev Soc Bras Med Trop **37:**476–479. http://dx.doi.org/10.1590/S0037-86822004000600009.
15. **Baisley KJ, Watts DM, Munstermann LE, Wilson ML.** 1998. Epidemiology of endemic Oropouche virus transmission in upper Amazonian Peru. Am J Trop Med Hyg **59:**710–716.
16. **Smith GC, Francy DB.** 1991. Laboratory studies of a Brazilian strain of *Aedes albopictus* as a potential vector of Mayaro and Oropouche viruses. J Am Mosq Control Assoc **7:**89–93.
17. **Mouraao MP, Bastos MS, Gimaqu JB, Mota BR, Souza GS, Grimmer GH, Galusso ES, Arruda E, Figueiredo LT.** 2009. Oropouche fever outbreak, Manaus, Brazil, 2007-2008. Emerg Infect Dis **15:**2063–2064. http://dx.doi.org/10.3201/eid1512.090917.
18. **Bastos Mde S, Figueiredo LT, Naveca FG, Monte RL, Lessa N, Pinto de Figueiredo RM, Gimaque JB, Pivoto Joao G, Ramasawmy R, Mourao MP.** 2012. Identification of Oropouche orthobunyavirus in the cerebrospinal fluid of three patients in the Amazonas, Brazil. Am J Trop Med Hyg **86:**732–735. http://dx.doi.org/10.4269/ajtmh.2012.11-0485.
19. **Bastos MS, Lessa N, Naveca FG, Monte RL, Braga WS, Figueiredo LT, Ramasawmy R, Mourao MP.** 2014. Detection of herpesvirus, enterovirus,

and arbovirus infection in patients with suspected central nervous system viral infection in the Western Brazilian Amazon. J Med Virol **86:**1522–1527. http://dx.doi.org/10.1002/jmv.23953.

20. **Pinheiro FP, Rocha AG, Freitas RB, Ohana BA, Travassos da Rosa AP, Rogerio JS, Linhares AC.** 1982. Meningitis associated with Oropouche virus infections. Rev Inst Med Trop Sao Paulo **24:**246–251.
21. **Rodrigues AH, Santos RI, Arisi GM, Bernardes ES, Silva ML, Rossi MA, Lopes MB, Arruda E.** 2011. Oropouche virus experimental infection in the golden hamster (*Mesocrisetus auratus*). Virus Res **155:**35–41. http://dx.doi.org/10.1016/j.virusres.2010.08.009.
22. **Santos RI, Almeida MF, Paula FE, Rodrigues AH, Saranzo AM, Paula AE, Silva ML, Correa VM, Acrani GO, Neder L, Arruda E.** 2012. Experimental infection of suckling mice by subcutaneous inoculation with Oropouche virus. Virus Res **170:**25–33. http://dx.doi.org/10.1016/j.virusres.2012.07.006.
23. **Santos RI, Bueno-Junior LS, Ruggiero RN, Almeida MF, Silva ML, Paula FE, Correa VM, Arruda E.** 2014. Spread of Oropouche virus into the central nervous system in mouse. Viruses **6:**3827–3836. http://dx.doi.org/10.3390/v6103827.
24. **Pagni S, Fernandez-Sesma A.** 2012. Evasion of the human innate immune system by dengue virus. Immunol Res **54:**152–159. http://dx.doi.org/10.1007/s12026-012-8334-2.
25. **Couderc T, Chretien F, Schilte C, Disson O, Brigitte M, Guivel-Benhassine F, Touret Y, Barau G, Cayet N, Schuffenecker I, Despres P, Arenzana-Seisdedos F, Michault A, Albert ML, Lecuit M.** 2008. A mouse model for Chikungunya: young age and inefficient type-I interferon signaling are risk factors for severe disease. PLoS Pathog **4:**e29. http://dx.doi.org/10.1371/journal.ppat.0040029.
26. **Diamond MS, Gale M, Jr.** 2012. Cell-intrinsic innate immune control of West Nile virus infection. Trends Immunol **33:**522–530. http://dx.doi.org/10.1016/j.it.2012.05.008.
27. **Jensen S, Thomsen AR.** 2012. Sensing of RNA viruses: a review of innate immune receptors involved in recognizing RNA virus invasion. J Virol **86:**2900–2910. http://dx.doi.org/10.1128/JVI.05738-11.
28. **Ramos HJ, Gale M, Jr.** 2011. RIG-I like receptors and their signaling crosstalk in the regulation of antiviral immunity. Curr Opin Virol **1:**167–176. http://dx.doi.org/10.1016/j.coviro.2011.04.004.
29. **Wilkins C, Gale M, Jr.** 2010. Recognition of viruses by cytoplasmic sensors. Curr Opin Immunol **22:**41–47. http://dx.doi.org/10.1016/j.coi.2009.12.003.
30. **Adachi O, Kawai T, Takeda K, Matsumoto M, Tsutsui H, Sakagami M, Nakanishi K, Akira S.** 1998. Targeted disruption of the MyD88 gene results in loss of IL-1- and IL-18-mediated function. Immunity **9:**143–150. http://dx.doi.org/10.1016/S1074-7613(00)80596-8.
31. **Schoggins JW.** 2014. Interferon-stimulated genes: roles in viral pathogenesis. Curr Opin Virol **6:**40–46. http://dx.doi.org/10.1016/j.coviro.2014.03.006.
32. **Taylor KG, Peterson KE.** 2014. Innate immune response to La Crosse virus infection. J Neurovirol **20:**150–156. http://dx.doi.org/10.1007/s13365-013-0186-6.
33. **Bridgen A, Weber F, Fazakerley JK, Elliott RM.** 2001. Bunyamwera bunyavirus nonstructural protein NSs is a nonessential gene product that contributes to viral pathogenesis. Proc Natl Acad Sci U S A **98:**664–669. http://dx.doi.org/10.1073/pnas.98.2.664.
34. **Varela M, Schnettler E, Caporale M, Murgia C, Barry G, McFarlane M, McGregor E, Piras IM, Shaw A, Lamm C, Janowicz A, Beer M, Glass M, Herder V, Hahn K, Baumgartner W, Kohl A, Palmarini M.** 2013. Schmallenberg virus pathogenesis, tropism and interaction with the innate immune system of the host. PLoS Pathog **9:**e1003133. http://dx.doi.org/10.1371/journal.ppat.1003133.
35. **Blakqori G, Delhaye S, Habjan M, Blair CD, Sanchez-Vargas I, Olson KE, Attarzadeh-Yazdi G, Fragkoudis R, Kohl A, Kalinke U, Weiss S, Michiels T, Staeheli P, Weber F.** 2007. La Crosse bunyavirus nonstructural protein NSs serves to suppress the type I interferon system of mammalian hosts. J Virol **81:**4991–4999. http://dx.doi.org/10.1128/JVI.01933-06.
36. **Hefti HP, Frese M, Landis H, Di Paolo C, Aguzzi A, Haller O, Pavlovic J.** 1999. Human MxA protein protects mice lacking a functional alpha/beta interferon system against La Crosse virus and other lethal viral infections. J Virol **73:**6984–6991.
37. **Weber F, Bridgen A, Fazakerley JK, Streitenfeld H, Kessler N, Randall RE, Elliott RM.** 2002. Bunyamwera bunyavirus nonstructural protein NSs counteracts the induction of alpha/beta interferon. J Virol **76:**7949–7955. http://dx.doi.org/10.1128/JVI.76.16.7949-7955.2002.
38. **Lorenzo G, Martin-Folgar R, Hevia E, Boshra H, Brun A.** 2010. Protection against lethal Rift Valley fever virus (RVFV) infection in transgenic IFNAR(−/−) mice induced by different DNA vaccination regimens. Vaccine **28:**2937–2944. http://dx.doi.org/10.1016/j.vaccine.2010.02.018.
39. **Zivcec M, Safronetz D, Scott D, Robertson S, Ebihara H, Feldmann H.** 2013. Lethal Crimean-Congo hemorrhagic fever virus infection in interferon alpha/beta receptor knockout mice is associated with high viral loads, proinflammatory responses, and coagulopathy. J Infect Dis **207:**1909–1921. http://dx.doi.org/10.1093/infdis/jit061.
40. **Mukherjee P, Woods TA, Moore RA, Peterson KE.** 2013. Activation of the innate signaling molecule MAVS by bunyavirus infection upregulates the adaptor protein SARM1, leading to neuronal death. Immunity **38:**705–716. http://dx.doi.org/10.1016/j.immuni.2013.02.013.
41. **Kohl A, Clayton RF, Weber F, Bridgen A, Randall RE, Elliott RM.** 2003. Bunyamwera virus nonstructural protein NSs counteracts interferon regulatory factor 3-mediated induction of early cell death. J Virol **77:**7999–8008. http://dx.doi.org/10.1128/JVI.77.14.7999-8008.2003.
42. **Bupp K, Gonzalez-Scarano F.** 1998. Pseudotype formation with La Crosse virus glycoproteins. J Gen Virol **79**(Part 4)**:**667–671.
43. **Pekosz A, Griot C, Stillmock K, Nathanson N, Gonzalez-Scarano F.** 1995. Protection from La Crosse virus encephalitis with recombinant glycoproteins: role of neutralizing anti-G1 antibodies. J Virol **69:**3475–3481.
44. **National Research Council.** 2011. Guide for the care and use of laboratory animals, 8th ed. National Academies Press, Washington, DC.
45. **Sato M, Suemori H, Hata N, Asagiri M, Ogasawara K, Nakao K, Nakaya T, Katsuki M, Noguchi S, Tanaka N, Taniguchi T.** 2000. Distinct and essential roles of transcription factors IRF-3 and IRF-7 in response to viruses for IFN-alpha/beta gene induction. Immunity **13:**539–548. http://dx.doi.org/10.1016/S1074-7613(00)00053-4.
46. **Honda K, Yanai H, Negishi H, Asagiri M, Sato M, Mizutani T, Shimada N, Ohba Y, Takaoka A, Yoshida N, Taniguchi T.** 2005. IRF-7 is the master regulator of type-I interferon-dependent immune responses. Nature **434:**772–777. http://dx.doi.org/10.1038/nature03464.
47. **Daffis S, Suthar MS, Szretter KJ, Gale M, Jr, Diamond MS.** 2009. Induction of IFN-beta and the innate antiviral response in myeloid cells occurs through an IPS-1-dependent signal that does not require IRF-3 and IRF-7. PLoS Pathog **5:**e1000607. http://dx.doi.org/10.1371/journal.ppat.1000607.
48. **Suthar MS, Ramos HJ, Brassil MM, Netland J, Chappell CP, Blahnik G, McMillan A, Diamond MS, Clark EA, Bevan MJ, Gale M, Jr.** 2012. The RIG-I-like receptor LGP2 controls CD8(+) T cell survival and fitness. Immunity **37:**235–248. http://dx.doi.org/10.1016/j.immuni.2012.07.004.
49. **Takaoka A, Mitani Y, Suemori H, Sato M, Yokochi T, Noguchi S, Tanaka N, Taniguchi T.** 2000. Cross talk between interferon-gamma and -alpha/beta signaling components in caveolar membrane domains. Science **288:**2357–2360. http://dx.doi.org/10.1126/science.288.5475.2357.
50. **Gitlin L, Barchet W, Gilfillan S, Cella M, Beutler B, Flavell RA, Diamond MS, Colonna M.** 2006. Essential role of mda-5 in type I IFN responses to polyriboinosinic:polyribocytidylic acid and encephalomyocarditis picornavirus. Proc Natl Acad Sci U S A **103:**8459–8464. http://dx.doi.org/10.1073/pnas.0603082103.
51. **Pinto AK, Ramos HJ, Wu X, Aggarwal S, Shrestha B, Gorman M, Kim KY, Suthar MS, Atkinson JP, Gale M, Jr, Diamond MS.** 2014. Deficient IFN signaling by myeloid cells leads to MAVS-dependent virus-induced sepsis. PLoS Pathog **10:**e1004086. http://dx.doi.org/10.1371/journal.ppat.1004086.
52. **Lazear HM, Lancaster A, Wilkins C, Suthar MS, Huang A, Vick SC, Clepper L, Thackray L, Brassil MM, Virgin HW, Nikolich-Zugich J, Moses AV, Gale M, Jr, Fruh K, Diamond MS.** 2013. IRF-3, IRF-5, and IRF-7 coordinately regulate the type I IFN response in myeloid dendritic cells downstream of MAVS signaling. PLoS Pathog **9:**e1003118. http://dx.doi.org/10.1371/journal.ppat.1003118.
53. **Livak KJ, Schmittgen TD.** 2001. Analysis of relative gene expression data using real-time quantitative PCR and the 2(-Delta Delta C(T)) method. Methods **25:**402–408. http://dx.doi.org/10.1006/meth.2001.1262.
54. **Kato H, Takeuchi O, Sato S, Yoneyama M, Yamamoto M, Matsui K, Uematsu S, Jung A, Kawai T, Ishii KJ, Yamaguchi O, Otsu K, Tsujimura T, Koh CS, Reis e Sousa C, Matsuura Y, Fujita T, Akira S.** 2006. Differential roles of MDA5 and RIG-I helicases in the recognition of RNA viruses. Nature **441:**101–105. http://dx.doi.org/10.1038/nature04734.
55. **Soldan SS, Plassmeyer ML, Matukonis MK, Gonzalez-Scarano F.** 2005. La Crosse virus nonstructural protein NSs counteracts the effects of short interfering RNA. J Virol **79:**234–244. http://dx.doi.org/10.1128/JVI.79.1.234-244.2005.

56. **Grandvaux N, Servant MJ, ten Oever B, Sen GC, Balachandran S, Barber GN, Lin R, Hiscott J.** 2002. Transcriptional profiling of interferon regulatory factor 3 target genes: direct involvement in the regulation of interferon-stimulated genes. J Virol **76:**5532–5539. http://dx.doi.org/10.1128/JVI.76.11.5532-5539.2002.
57. **Prinz M, Schmidt H, Mildner A, Knobeloch KP, Hanisch UK, Raasch J, Merkler D, Detje C, Gutcher I, Mages J, Lang R, Martin R, Gold R, Becher B, Bruck W, Kalinke U.** 2008. Distinct and nonredundant *in vivo* functions of IFNAR on myeloid cells limit autoimmunity in the central nervous system. Immunity **28:**675–686. http://dx.doi.org/10.1016/j.immuni.2008.03.011.
58. **Diamond MS, Kinder M, Matsushita H, Mashayekhi M, Dunn GP, Archambault JM, Lee H, Arthur CD, White JM, Kalinke U, Murphy KM, Schreiber RD.** 2011. Type I interferon is selectively required by dendritic cells for immune rejection of tumors. J Exp Med **208:**1989–2003. http://dx.doi.org/10.1084/jem.20101158.
59. **Lazear HM, Pinto AK, Vogt MR, Gale M, Jr, Diamond MS.** 2011. Beta interferon controls West Nile virus infection and pathogenesis in mice. J Virol **85:**7186–7194. http://dx.doi.org/10.1128/JVI.00396-11.
60. **Honda K, Takaoka A, Taniguchi T.** 2006. Type I interferon [corrected] gene induction by the interferon regulatory factor family of transcription factors. Immunity **25:**349–360. http://dx.doi.org/10.1016/j.immuni.2006.08.009.
61. **Izaguirre A, Barnes BJ, Amrute S, Yeow WS, Megjugorac N, Dai J, Feng D, Chung E, Pitha PM, Fitzgerald-Bocarsly P.** 2003. Comparative analysis of IRF and IFN-alpha expression in human plasmacytoid and monocyte-derived dendritic cells. J Leukoc Biol **74:**1125–1138. http://dx.doi.org/10.1189/jlb.0603255.
62. **Schilte C, Buckwalter MR, Laird ME, Diamond MS, Schwartz O, Albert ML.** 2012. Cutting edge: independent roles for IRF-3 and IRF-7 in hematopoietic and nonhematopoietic cells during host response to Chikungunya infection. J Immunol **188:**2967–2971. http://dx.doi.org/10.4049/jimmunol.1103185.
63. **Brien JD, Daffis S, Lazear HM, Cho H, Suthar MS, Gale M, Jr, Diamond MS.** 2011. Interferon regulatory factor-1 (IRF-1) shapes both innate and CD8(+) T cell immune responses against West Nile virus infection. PLoS Pathog **7:**e1002230. http://dx.doi.org/10.1371/journal.ppat.1002230.
64. **Fujita T, Kimura Y, Miyamoto M, Barsoumian EL, Taniguchi T.** 1989. Induction of endogenous IFN-alpha and IFN-beta genes by a regulatory transcription factor, IRF-1. Nature **337:**270–272.
65. **Miyamoto M, Fujita T, Kimura Y, Maruyama M, Harada H, Sudo Y, Miyata T, Taniguchi T.** 1988. Regulated expression of a gene encoding a nuclear factor, IRF-1, that specifically binds to IFN-beta gene regulatory elements. Cell **54:**903–913. http://dx.doi.org/10.1016/S0092-8674(88)91307-4.
66. **Thackray LB, Shrestha B, Richner JM, Miner JJ, Pinto AK, Lazear HM, Gale M, Jr, Diamond MS.** 2014. Interferon regulatory factor 5-dependent immune responses in the draining lymph node protect against West Nile virus infection. J Virol **88:**11007–11021. http://dx.doi.org/10.1128/JVI.01545-14.
67. **Zellweger RM, Shresta S.** 2014. Mouse models to study dengue virus immunology and pathogenesis. Front Immunol **5:**151. http://dx.doi.org/10.3389/fimmu.2014.00151.
68. **Carvalho VL, Nunes MR, da Silva EV, Vieira CM, Gomes M, Casseb SM, Rodrigues SG, Nunes-Neto JP, Quaresma JA, Vasconcelos PF.** 2009. Genetic characterization of orthobunyavirus Melao, strains BE AR633512 and BE AR8033, and experimental infection in golden hamsters (*Mesocricetus auratus*). J Gen Virol **90:**223–233. http://dx.doi.org/10.1099/vir.0.002360-0.
69. **Camini FC, Almeida LT, Bernardes CS, Silva M, Pedrosa ML, Costa DC, de Lima WG, do Amaral Pinto C, Ferreira PC, de Magalhaes JC, de Brito Magalhaes CL.** 2014. Caraparu virus induces damage and alterations in antioxidant defenses in the liver of BALB/c mice after subcutaneous infection. Arch Virol **159:**2621–2632. http://dx.doi.org/10.1007/s00705-014-2123-2.
70. **Cervantes-Barragan L, Kalinke U, Zust R, Konig M, Reizis B, Lopez-Macias C, Thiel V, Ludewig B.** 2009. Type I IFN-mediated protection of macrophages and dendritic cells secures control of murine coronavirus infection. J Immunol **182:**1099–1106. http://dx.doi.org/10.4049/jimmunol.182.2.1099.
71. **Zust R, Toh YX, Valdes I, Cerny D, Heinrich J, Hermida L, Marcos E, Guillen G, Kalinke U, Shi PY, Fink K.** 2014. Type I interferon signals in macrophages and dendritic cells control dengue virus infection: implications for a new mouse model to test dengue vaccines. J Virol **88:**7276–7285. http://dx.doi.org/10.1128/JVI.03827-13.
72. **Schilte C, Couderc T, Chretien F, Sourisseau M, Gangneux N, Guivel-Benhassine F, Kraxner A, Tschopp J, Higgs S, Michault A, Arenzana-Seisdedos F, Colonna M, Peduto L, Schwartz O, Lecuit M, Albert ML.** 2010. Type I IFN controls Chikungunya virus via its action on nonhematopoietic cells. J Exp Med **207:**429–442. http://dx.doi.org/10.1084/jem.20090851.
73. **Taylor KG, Woods TA, Winkler CW, Carmody AB, Peterson KE.** 2014. Age-dependent myeloid dendritic cell responses mediate resistance to La Crosse virus-induced neurological disease. J Virol **88:**11070–11079. http://dx.doi.org/10.1128/JVI.01866-14.
74. **Frias-Staheli N, Giannakopoulos NV, Kikkert M, Taylor SL, Bridgen A, Paragas J, Richt JA, Rowland RR, Schmaljohn CS, Lenschow DJ, Snijder EJ, Garcia-Sastre A, Virgin HW, IV.** 2007. Ovarian tumor domain-containing viral proteases evade ubiquitin- and ISG15-dependent innate immune responses. Cell Host Microbe **2:**404–416. http://dx.doi.org/10.1016/j.chom.2007.09.014.
75. **Blakqori G, Weber F.** 2005. Efficient cDNA-based rescue of La Crosse bunyaviruses expressing or lacking the nonstructural protein NSs. J Virol **79:**10420–10428. http://dx.doi.org/10.1128/JVI.79.16.10420-10428.2005.
76. **Eifan S, Schnettler E, Dietrich I, Kohl A, Blomstrom AL.** 2013. Non-structural proteins of arthropod-borne bunyaviruses: roles and functions. Viruses **5:**2447–2468. http://dx.doi.org/10.3390/v5102447.
77. **Ogawa Y, Sugiura K, Kato K, Tohya Y, Akashi H.** 2007. Rescue of Akabane virus (family Bunyaviridae) entirely from cloned cDNAs by using RNA polymerase I. J Gen Virol **88:**3385–3390. http://dx.doi.org/10.1099/vir.0.83173-0.
78. **Acrani GO, Tilston-Lunel NL, Spiegel M, Weidemann M, Dilcher M, da Silva DE, Nunes MR, Elliott RM.** 9 December 2014. Establishment of a minigenome system for Oropouche orthobunyavirus reveals the S genome segment to be significantly longer than previously reported. J Gen Virol. http://dx.doi.org/10.1099/jgv.0.000005._.
79. **Aguirre S, Maestre AM, Pagni S, Patel JR, Savage T, Gutman D, Maringer K, Bernal-Rubio D, Shabman RS, Simon V, Rodriguez-Madoz JR, Mulder LC, Barber GN, Fernandez-Sesma A.** 2012. DENV inhibits type I IFN production in infected cells by cleaving human STING. PLoS Pathog **8:**e1002934. http://dx.doi.org/10.1371/journal.ppat.1002934.
80. **Ashour J, Laurent-Rolle M, Shi PY, Garcia-Sastre A.** 2009. NS5 of dengue virus mediates STAT2 binding and degradation. J Virol **83:**5408–5418. http://dx.doi.org/10.1128/JVI.02188-08.
81. **Ashour J, Morrison J, Laurent-Rolle M, Belicha-Villanueva A, Plumlee CR, Bernal-Rubio D, Williams KL, Harris E, Fernandez-Sesma A, Schindler C, Garcia-Sastre A.** 2010. Mouse STAT2 restricts early dengue virus replication. Cell Host Microbe **8:**410–421. http://dx.doi.org/10.1016/j.chom.2010.10.007.
82. **Yu CY, Chang TH, Liang JJ, Chiang RL, Lee YL, Liao CL, Lin YL.** 2012. Dengue virus targets the adaptor protein MITA to subvert host innate immunity. PLoS Pathog **8:**e1002780. http://dx.doi.org/10.1371/journal.ppat.1002780.
83. **Silva AF, Arruda E.** 2008. PCR em tempo real para detecção específica de RNAS (+) e (−) vírus oropouche. USP, Ribeirao Preto, Brazil.
84. **Daffis S, Samuel MA, Keller BC, Gale M, Jr, Diamond MS.** 2007. Cell-specific IRF-3 responses protect against West Nile virus infection by interferon-dependent and -independent mechanisms. PLoS Pathog **3:**e106. http://dx.doi.org/10.1371/journal.ppat.0030106.